Thio-2 Inhibits Key Signaling Pathways Required for the Development and Progression of Castration-resistant Prostate Cancer

Antje Neeb[1], Ines Figueiredo[1], Denisa Bogdan[1], Laura Cato[2], Jutta Stober[3], Juan M. Jiménez-Vacas[1], Victor Gourain[3], Irene I. Lee[2], Rebecca Seeger[3], Claudia Muhle-Goll[4], Bora Gurel[1], Jonathan Welti[1], Daniel Nava Rodrigues[1], Jan Rekowski[1], Xintao Qiu[2], Yija Jiang[2], Patrizio Di Micco[1,5], Borja Mateos[6], Stasė Bielskutė[6], Ruth Riisnaes[1], Ana Ferreira[1], Susana Miranda[1], Mateus Crespo[1], Lorenzo Buroni[1], Jian Ning[1], Suzanne Carreira[1], Stefan Bräse[7], Nicole Jung[7], Simone Gräßle[7], Amanda Swain[1], Xavier Salvatella[6,8], Stephen R. Plymate[9,10], Bissan Al-Lazikani[5], Henry W. Long[2], Wei Yuan[1], Myles Brown[2], Andrew C.B. Cato[3], Johann S. de Bono[1,11], and Adam Sharp[1,11]

ABSTRACT

Therapies that abrogate persistent androgen receptor (AR) signaling in castration-resistant prostate cancer (CRPC) remain an unmet clinical need. The N-terminal domain of the AR that drives transcriptional activity in CRPC remains a challenging therapeutic target. Herein we demonstrate that BCL-2–associated athanogene-1 (BAG-1) mRNA is highly expressed and associates with signaling pathways, including AR signaling, that are implicated in the development and progression of CRPC. In addition, interrogation of geometric and physiochemical properties of the BAG domain of BAG-1 isoforms identifies it to be a tractable but challenging drug target. Furthermore, through BAG-1 isoform mouse knockout studies, we confirm that BAG-1 isoforms regulate hormone physiology and that therapies targeting the BAG domain will be associated with limited "on-target" toxicity. Importantly, the postulated inhibitor of BAG-1 isoforms, Thio-2, suppressed AR signaling and other important pathways implicated in the development and progression of CRPC to reduce the growth of treatment-resistant prostate cancer cell lines and patient-derived models. However, the mechanism by which Thio-2 elicits the observed phenotype needs further elucidation as the genomic abrogation of BAG-1 isoforms was unable to recapitulate the Thio-2–mediated phenotype. Overall, these data support the interrogation of related compounds with improved drug-like properties as a novel therapeutic approach in CRPC, and further highlight the clinical potential of treatments that block persistent AR signaling which are currently undergoing clinical evaluation in CRPC.

Introduction

Prostate cancer is the most commonly diagnosed noncutaneous malignancy in men and is a leading cause of male mortality (1). Despite the development of novel hormonal therapies targeting the androgen receptor (AR), such as abiraterone, enzalutamide, apalutamide, and darolutamide, that have improved the outcome for patients with advanced castration-sensitive prostate cancer (CSPC) and castration-resistant prostate cancer (CRPC), primary and secondary resistance to therapy remains inevitable (2, 3). Treatment resistance is driven, in part, by persistent AR signaling associated with the emergence of AR amplification, AR activating mutations, and constitutively active AR splice variants (3–7). The development of novel therapies that block persistent AR signaling is an urgent unmet clinical need.

One attractive therapeutic strategy is to target molecular co-chaperones, such as BAG-1 (BCL-2–associated athanogene-1), that have been reported to bind and enhance AR activity. BAG-1 interacts with a wide range of molecular targets to regulate multiple cellular pathways (including apoptosis, proliferation, metastasis, and nuclear hormone receptor transactivation) important for the development and progression of cancer (8–10). Three major isoforms, BAG-1L (50 kDa), BAG-1M (46 kDa), and BAG-1S (36 kDa), exist in humans and are generated through alternative initiation of translation from a single mRNA (11). Consistent with this, BAG-1L has a unique N-terminus which contains a nuclear localization sequence and is predominantly localized within the nucleus, supporting its interaction with the AR, whereas the other isoforms (BAG-1M and BAG-1S) are found in both the nucleus and cytoplasm (8–10). All BAG-1 isoforms share a common C-terminus, which contains the highly conserved BAG domain, critical for the interaction between BAG-1 isoforms and

[1]Institute of Cancer Research, London, United Kingdom. [2]Dana-Farber Cancer Institute, Boston, Massachusetts. [3]Karlsruhe Institute of Technology (KIT), Institute for Biological and Chemical Systems – Biological Information Processing (IBCS-BIP), Eggenstein-Leopoldshafen, Germany. [4]Karlsruhe Institute of Technology (KIT), Institute for Biological Interfaces 4 (IBG-4), Eggenstein-Leopoldshafen, Germany. [5]MD Anderson Cancer Centre, Houston, Texas. [6]Institute for Research in Biomedicine, The Barcelona Institute of Science and Technology, Barcelona, Spain. [7]Karlsruhe Institute of Technology (KIT), Institute of Biological and Chemical Systems – Functional Molecular Systems (IBCS-FMS), Eggenstein-Leopoldshafen, Germany. [8]Catalan Institution for Research and Advanced Studies, Barcelona, Spain. [9]University of Washington, Seattle, Washington. [10]Geriatrics Research, Education and Clinical Center, VAPSHCS, Seattle, Washington. [11]Royal Marsden NHS Foundation Trust, London, United Kingdom.

A. Sharp and J.S. de Bono contributed as co-senior authors to this article.

Corresponding Author: Adam Sharp, Institute of Cancer Research, 15 Cotswold Rd, Sutton, Surrey, SM2 5NG, London, United Kingdom. E-mail: adam.sharp@icr.ac.uk

Mol Cancer Ther 2024;23:791–808

doi: 10.1158/1535-7163.MCT-23-0354

the heat shock chaperones, HSC70/HSP70 (12–14). Importantly, the BAG-1:HSC70/HSP70 interaction is reported to be critical for BAG-1 function and therefore therapies targeting this interaction are an attractive strategy to overcome BAG-1 function in cancer (8–10, 15–22).

BAG-1L plays a critical role in transactivation of the AR and nuclear BAG-1 protein expression correlates with important clinical characteristics in prostate cancer (15–18, 23–25). Through its C-terminal BAG domain, BAG-1L binds to the AR N-terminal domain (NTD), leading to receptor transactivation (15–18). Consistent with this, loss of BAG-1L abrogates AR signaling and reduces prostate cancer growth (15). In addition, expression of nuclear BAG-1 correlates with worse outcome from AR targeting therapies in patients with CRPC (15). Moreover, mutagenesis studies demonstrated that specific amino acid residues within the BAG domain of BAG-1L are critical for the BAG-1L–AR interaction and AR transactivation (15). Finally, Thio-2, a tool compound that has been predicted to bind the BAG domain within BAG-1 isoforms through *in silico* docking experiments, and more recently A4B17 and X15695, have been reported to inhibit BAG-1L–mediated AR NTD transactivation (15, 26–29). Taken together, these data support targeting the BAG domain of BAG-1 isoforms as an attractive therapeutic strategy to overcome persistent AR signaling in CRPC.

Herein we confirm that BAG-1 mRNA is highly expressed and associates with signaling pathways critical for the development and progression of CRPC. In addition, we report that the BAG domain provides a tractable drug target, and that BAG-1 mouse knockout (KO) studies indicate that BAG-1 isoforms may mediate hormone physiology and targeting the BAG domain should be associated with minimal "on-target" toxicity. Moreover, we show that Thio-2 which is predicted to bind the BAG domain, suppresses AR activity and other key signaling pathways, to inhibit the growth of prostate cancer cell lines and patient-derived models. The Thio-2 phenotype was not copied by either BAG-1 isoform knockdown or KO, suggesting, that in these studies, the mechanism of action of Thio-2 was not mediated through BAG-1 isoforms. Taken together, these data support the interrogation of related compounds, with improved drug-like properties, as a novel therapeutic strategy for CRPC.

Materials and Methods

CRPC patient transcriptome analyses

CRPC transcriptomes from the Stand Up To Cancer/Prostate Cancer Foundation (SU2C/PCF) cohort were downloaded and reanalyzed (30, 31). CRPC transcriptomes from the Institute of Cancer Research/Royal Marsden Hospital (ICR/RMH) cohort were reanalyzed (32). Paired-end transcriptome sequencing reads for each of the SU2C/PCF ($n = 159$) and ICR/RMH ($n = 95$) cohorts were aligned to the human reference genome (GRCh37/hg19) using Tophat2 (v2.0.7). Gene expression, fragments per kilobase of transcript per million mapped reads (FPKM), was calculated using Cufflinks. The top expressed genes ($n = 15{,}000$) were analyzed for each cohort, respectively. Gene set enrichment analysis (GSEA) was performed using the preranked algorithm from GSEA software (v4.1.0). The top genes were ranked from high to low using the Spearman correlation coefficient between each gene's expression (FPKM) and BAG-1 expression (FPKM), and subsequently used in analysis. Results were obtained using Molecular Signatures Database hallmark gene collection (33).

canSAR platform

Briefly, the algorithm identifies up to 10 cavities on a three-dimensional (3D) structure and measures approximately 30 geometric and physicochemical properties for each of these cavities to determine ligandability. The tools and methodologies used are available at our online canSAR platform (34–36). Because proteins are mobile, and this mobility affects the formation of druggable cavities, we performed Monte Carlo simulations to explore limited movements of each structure. The simulations were performed using the CONCOORD method (37). Yamber2, Van der Waals and CONCOORD default bond/angle were set as parameters. A total of 449 alternative structures were shaped (at least 10 structures for each of the 44 original structures; Supplementary Table S1) and all cavities identified were assessed for ligandability by canSAR algorithm as described above.

BAG-1 exon 1 and exon 2 KO mice

Studies with BAG-1 KO mice were performed at the Karlsruhe Institute of Technology (KIT), Germany according to European and German statutory regulations and approved by the Regierungspräsidium Karlsruhe, Germany. BAG-1 exon 1 deleted KO mice were kindly provided by Michael Sendtner, Institute for Clinical Neurobiology, University of Wuerzburg, Germany (38). BAG-1 exon 2 deleted KO mice [Bag1tm1a(EUCOMM)Hmgu] were provided by the Infrafrontier European Mouse Mutant Archive. Animals were bred using conventional breeding methods, body weight was measured weekly. At the age of 3 months, mice were culled by cardiac puncture. Serum was isolated and testosterone content was analyzed by radioimmunoassay (Bioscientia Healthcare GmbH). Subsequently, organs were taken, weighed, and fixed for immunohistochemistry (IHC) or snap frozen for protein and ribonucleic acid (RNA) preparation.

Microarray analyses (exon 1 BAG-1 KO mice)

Prostates from BAG-1 exon 1 deleted heterozygous and wild-type (WT) control mice castrated for 12 weeks were minced and subjected to total RNA extraction using TRIzol (Invitrogen) and the RNAeasy Mini purification kit (Qiagen). Biological triplicate RNAs were hybridized to a human U133 Plus 2.0 expression array (Affymetrix) at the Dana-Farber Cancer Institute Microarray Core Facility. Gene expression data were normalized and log-scaled using the RMA algorithm and the RefSeq probe definition (39, 40).

RNA extraction, qRT-PCR, and Western blotting

RNA extraction, qRT-PCR, and Western blot analysis were performed as per standard laboratory protocols. Specific details, and primary antibodies and TaqMan probes used, are detailed in Supplementary Tables S2 and S3, and Supplementary Materials and Methods.

IHC

For IHC studies, androgen receptor full-length (AR-FL) and AR splice variant-7 (AR-V7) IHC was performed as described previously (5). Pan-mouse-BAG-1 (panmoBAG-1, mouse, goat polyclonal, AF815, R&D Systems), mouse/human AR-FL [AR-FL, mouse/human, rabbit monoclonal, EPR1535 (2), Abcam] and pan-BAG-1 (panBAG-1, human, rabbit monoclonal, RM356, RevMAb) were all validated and optimized for IHC in this study. Specific details on the IHC assays developed and quantification are detailed in Supplementary Table S4.

RNA sequencing and analysis (BAG-1 KO mice)

From 1 μg of total RNA, we pulled down polyadenylated RNAs with poly-dT magnetic beads. We then prepared sequencing

libraries with the TrueSeq Stranded mRNA kit (Illumina) following manufacturer protocol. These libraries were sequenced in paired-end mode (2×50 cycles) with a Hiseq1500 sequencer (Illumina). Raw sequencing data were demultiplexed with Bcl2fastq (version 2.17.1.14, Illumina). Paired end raw reads in FASTQ format were aligned to the reference mouse genome (mm9) using RNA sequencing (RNA-seq) spliced read mapper TopHat (v2.0.7) with default settings. Differential gene expression and individual gene and transcript expression in units of FPKM were calculated using Cuffdiff (Cufflinks v2.2.1) with default settings. The expressed genes (median expression in either control or treatment samples > 0; $n = 17{,}459$) were ranked from high to low using the fold change ($\log_2$), and subsequently used for pathway analysis. Pathway analysis was performed using the GSEA preranked algorithm from GSEA software (v4.1.0). GSEA preranked results were obtained using the H collection of hallmark gene sets and the C2 collection of curated gene sets (MSigDB v7.1), with default parameters. H and C2 collections were previously mapped to mouse orthologs using the HGNC Comparison of Orthology Prediction tool (https://www.genenames.org/tools/hcop/).

Compounds

Enzalutamide was purchased from MedChemExpress. Thio-2 (compound A1B1) was synthesized as previously described and provided by N. Jung (author; ref. 27).

In vivo Thio-2 toxicity studies

Non–tumor-bearing NSG male mice were treated with vehicle [5% DMSO in 10% (w/v) HBC (2-hydroxypropyl-β-cyclodextrin) in 0.9% saline] or 15 mg/kg Thio-2 by once daily intraperitoneal injection for 5 days with daily weights. Following 5 days treatment, mice were sacrificed and organ (heart, kidney, testes, seminal vesicles, and prostate) weights were determined.

In vivo LNCaP short hairpin RNA clone and patient-derived xenograft studies

For LNCaP short hairpin RNA (shRNA) clone *in vivo* studies, NSG male mice were inoculated subcutaneously with LNCaP shRNA control or BAG-1 clones and growth was determined between days 16 and 27 once tumors were established. For CP50 patient-derived xenografts (PDX), fragments of CP50 tumors were grafted subcutaneously into NSG male mice and drug treatment commenced with vehicle [5% DMSO in 10% (w/v) HBC (2-hydroxypropyl-β-cyclodextrin) in 0.9% saline] or 15 mg/kg Thio-2 by once daily intraperitoneal injection when tumors reached a size of 300 to 400 mm^3. Mice were treated daily for 5 days (pharmacodynamic analyses) or 14 days (efficacy analyses). After treatment mice were sacrificed, and plasma and tumors were collected for pharmacodynamic analyses.

In vivo PDX serum PSA analyses

Serum was separated by 5 minutes centrifugation at 9,000 rpm from blood collected from mice by cardiac puncture under general terminal anesthesia after blood clotting was allowed to take place for 15 minutes. Serum PSA was analyzed in 1:100 diluted serum using the human PSA SimpleStep ELISA kit (Abcam) following the manufacturer's instructions.

Cell lines

All cell lines used in this study (except for LNCaP95 which were a kind gift from Drs. Alan K Meeker and Jun Luo) were obtained from ATCC and grown in recommended media at 37°C in 5% CO_2 as detailed in Supplementary Table S5. Cell lines were grown from early passages, tested for *Mycoplasma* using the VenorGem One Step PCR Kit (Cambio), and short tandem repeat profiled at regular intervals. LNCaP shRNA clones were developed as described previously, clone C2 (control shRNA) and clone 506 (BAG-1 shRNA) were used for this study (29, 41).

RNA-seq and analysis (cell line)

For LNCaP shRNA clone experiments, LNCaP shRNA clones were grown in full media (10% FBS) and three biological replicates used. For unstimulated LNCaP cell experiments, LNCaP cells were grown in full media (10% FBS) prior to treatment with vehicle (DMSO 0.1%) or 50 μmol/L Thio-2 for 17 hours. For stimulated LNCaP cell experiments, LNCaP cells were grown in starved media (10% charcoal-stripped serum) for 72 hours prior to treatment with vehicle (DMSO 0.1%) or 5 μmol/L Thio-2. Following 1-hour pretreatment with vehicle or 5 μmol/L Thio-2; cells were treated with vehicle (Ethanol 0.1%) or 10 nmol/L dihydrotestosterone (DHT) for 16 hours thereafter (17 hours total treatment). Following treatments, cells were harvested and lysed, and RNA was extracted using Qiagen RNAeasyPlus RNA extraction kit Mini as per manufacturer's instruction. RNA quality was analyzed using the Agilent Tapestation RNA ScreenTape. A total of 500 ng of total RNA from each sample was first used in the NEBNext rRNA Depletion Kit followed by the NEBNext Ultra II Directional RNA Library Prep Kit, according to the manufacturer's instructions. Library quality was confirmed using the Agilent Tapestation High Sensitivity DNA ScreenTape. The libraries were quantified and normalized by qPCR using the KAPA Library Quantification Kit (Roche). Library clustering was performed on a cBot with Illumina HiSeq PE Cluster Kit v3. The libraries were sequenced as paired-end 101 bp reads on an Illumina HiSeq 2500 with an Illumina HiSeq SBS Kit v3. Base calling and quality scoring were performed using Real-Time Analyses (version 1.18.64) and FASTQ file generation and demultiplexing using CASAVA. Paired end raw reads in FASTQ format were aligned to the reference human genome (GRCh37/hg19) using RNA-seq spliced read mapper TopHat (v2.1.0), with default settings. The library and mapping quality were assessed using Picard tools (http:// broadinstitute.github.io/picard). Differential gene expression was calculated using Cuffdiff (Cufflinks v2.2.1), with default settings. The expressed genes [median gene expression level (FPKM) in either control and Thio-2–treated samples > 0; number of genes = 25,635] were ranked from high to low using the fold change ($\log_2$), and subsequently used for pathway analysis. Pathway analysis was performed using the GSEA preranked algorithm from GSEA software (v4.1.0). GSEA Pre-ranked results were obtained using the H collection of Hallmark gene sets (MsigDB v7.0), with default parameters.

Chromatin immunoprecipitation sequencing and analysis

Briefly, chromatin immunoprecipitation sequencing (ChIP-seq) libraries were generated using the ThruPLEX DNA-seq kit (Rubicon Genomics) and were sequenced on the Illumina NextSeq 500 platform at the Molecular Biology Core Facility (Dana-Farber Cancer Institute). All samples were processed through the computational pipeline developed at the Dana-Farber Cancer Institute Center for Functional Cancer Epigenetics using primarily open-source programs (42, 43). Sequence tags were aligned with Burrows-Wheeler Aligner to build hg19 and uniquely mapped, nonredundant reads were retained. These reads were used to generate binding sites with model-based analysis of ChIP-Seq 2 (MACS v2.1.1.20160309), with a q-value (FDR) threshold of 0.01 (44, 45). A read per million normalized BedGraph signal track file generated by MACS2 is further converted to a

BigWig file with bedGraphToBigWig (46). Deeptools is used for the plots heat map (47).

siRNA

Cells were transiently transfected with small interfering RNA (siRNA) as indicated. All siRNA were ON-TARGETplus pools (Dharmacon; Horizon), listed in Supplementary Table S6. The siRNA was used along with RNAiMax transfection reagent (Thermo Fisher Scientific) as per manufacturer's instructions and incubated with cells as indicated.

Development of BAG-1 CRISPR KO 22Rv1 and LNCaP95 cells

22Rv1 and LNCaP95 BAG-1 CRISPR KO cells were developed following the manufacturers protocol. Briefly, 100,000 cells were

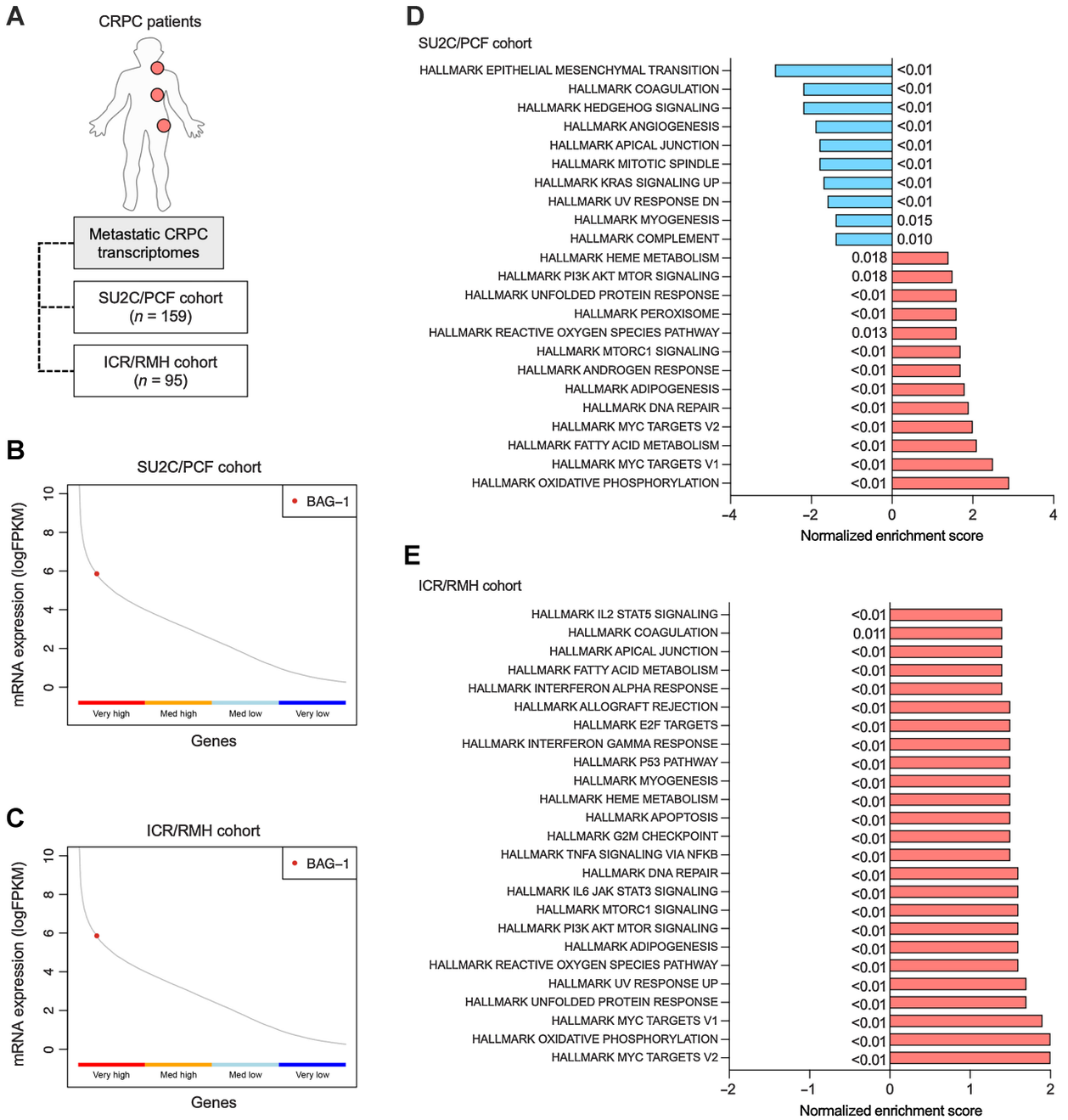

Figure 1.

BAG-1 is highly expressed and associates with signaling pathways critical for the development and progression of CRPC. **A,** Two independent CRPC patient transcriptome cohorts were used in this study. The SU2C/PCF patient cohort included RNA-seq on 159 CRPC biopsies and the ICR/RMH patient cohort included RNA-seq on 95 CRPC biopsies. SU2C/PCF (**B**) and ICR/RMH (**C**) CRPC transcriptome analyses for BAG-1 mRNA expression compared with the 20,000 highest expressed genes divided into very high (upper 25% expressed genes), medium high (50%–75% expressed genes), medium low (25%–50% expressed genes), and very low (lower 25% expressed genes). GESA shows BAG-1 mRNA levels association with hallmark pathways in SU2C/PCF (**D**) and ICR/RMH (**E**) cohorts. NESs and FDRs are shown. Hallmark pathways significantly (FDR ≤ 0.05) enriched and de-enriched with BAG-1 mRNA expression are shown.

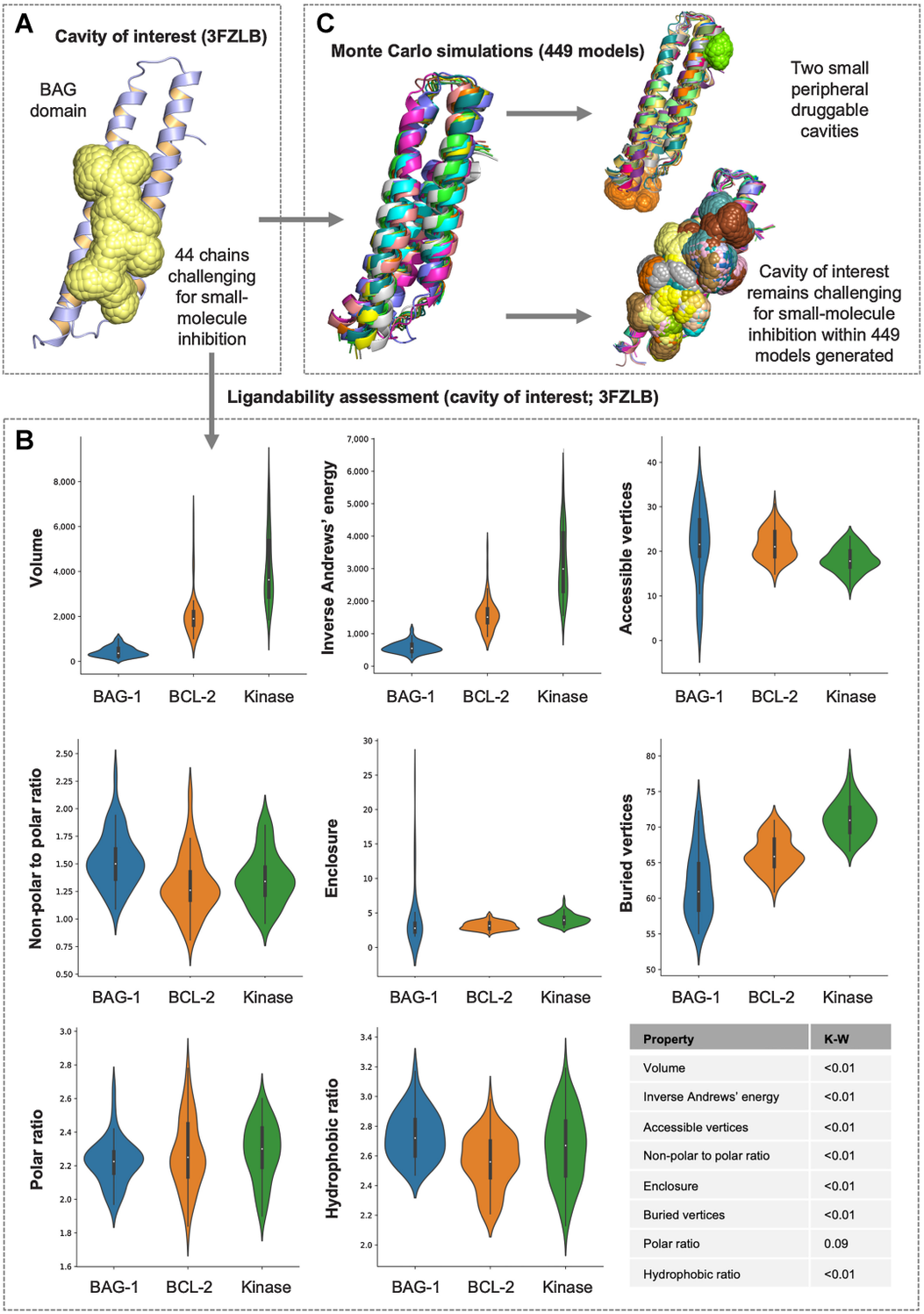

Figure 2.

Druggability assessment of the BAG domain of BAG-1. **A,** Visualization of the BAG domain cavity of interest identified by canSAR using the 44 3D HSC70-BAG domain structures available mapped onto the representative structure (PDB ID 3FZLB). The cavity of interest as volume surface (in yellow) is shown on the BAG domain (violet) of BAG-1. **B,** Key geometric and physicochemical parameters for the cavity of interest within the BAG domain (blue), a druggable protein–protein interaction (BCL-2; orange) and the druggable kinase ATP site (green) are shown as violin plots. *P* values were calculated using the Kruskal–Wallis (K-W) test. **C,** Monte Carlo simulations identified 449 models with 4,489 cavities for the original 44 3D HSC70-BAG domain structures.

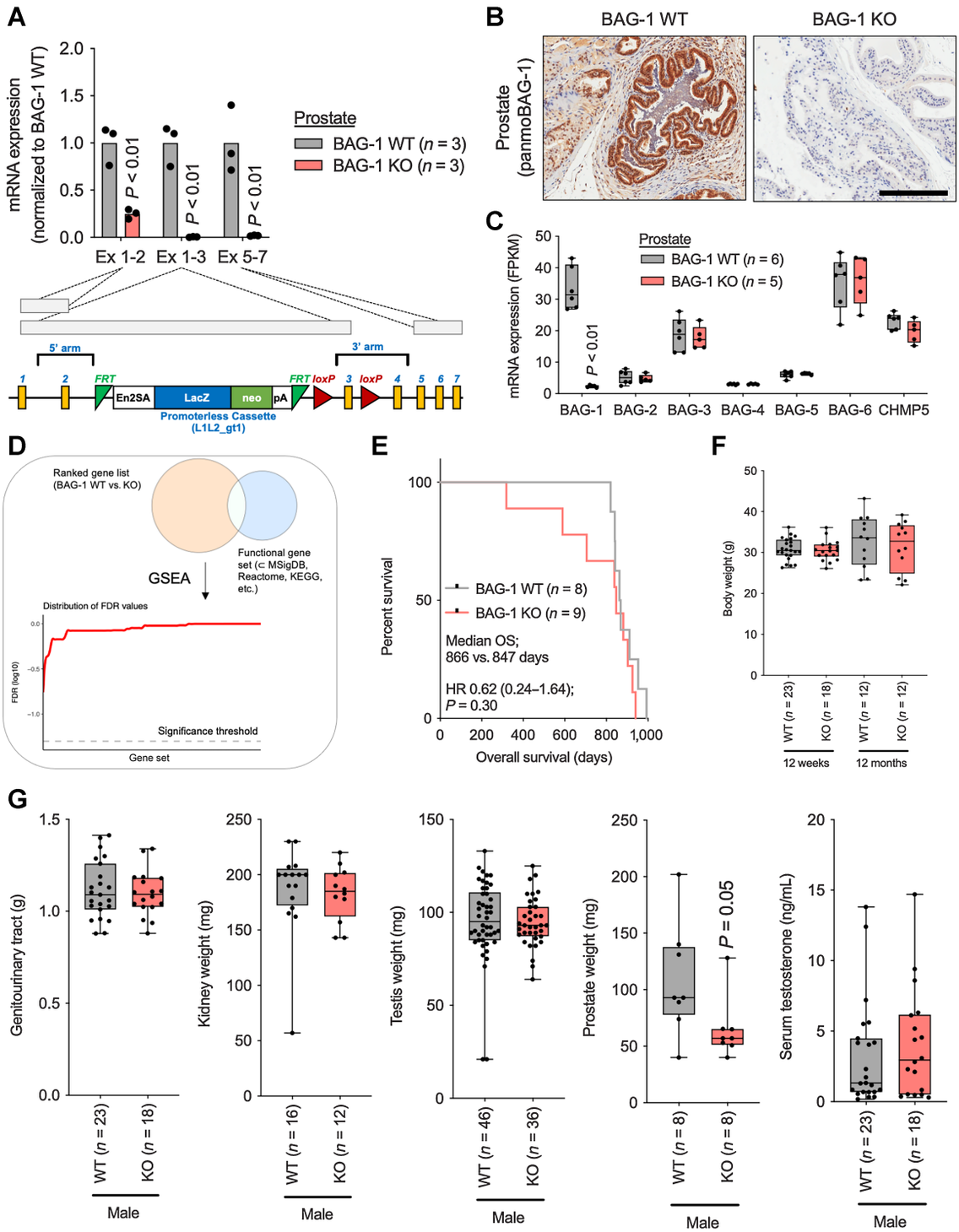

Figure 3.

BAG-1 KO male mice are fertile and viable with reduced prostate weight. **A,** BAG-1 KO mouse strain Bag1tm1a(EUCOMM)Hmgu was developed by the EUCOMM program by insertion of an artificial exon containing the coding sequence of beta-Geo, a fusion protein of beta-Galactosidase (LacZ) and neomycin (neo) followed by a stop codon and polyadenylation (pA) sequence between exon 2 and exon 3 flanked by Flp recognition sites disrupts the expression of the WT gene, replacing the endogenous BAG-1 expression by a fusion protein of the BAG-1 N-terminal sequence encoded in exon 1 and 2 and beta-Geo. Mouse prostates from BAG-1 KO and BAG-1 WT male mice were analyzed for BAG-1 mRNA (qRT-PCR) levels. BAG-1 exon 1 to 2 (Ex 1–2), exon 1 to 3 (Ex 1–3), and exon 5 to 7 (Ex 5–7) mRNA was quantified for BAG-1 KO (red bars; $n = 3$) and BAG-1 WT (gray bars; $n = 3$) mice. mRNA expression was calculated relative to mouse GAPDH and normalized to BAG-1 WT. Mean levels from three prostates are shown. *P* values were calculated for BAG-1 KO compared with BAG-1 WT mice using unpaired Student *t* test. *P* values ≤ 0.05 are shown. **B,** Prostates from BAG-1 KO mouse strain Bag1tm1a(EUCOMM)Hmgu and BAG-1 WT male mice were analyzed for mouse BAG-1 protein (IHC) levels. Representative micrographs of BAG-1 detection in mouse prostates by panmoBAG-1 antibody IHC are shown. Scale bar, 200 µm. (*Continued on the following page.*)

transfected with BAG-1 single-guide RNA (sgRNA; 6 μmol/L; Synthego) and Cas9 2NLS (0.67 μmol/L; Synthego) using the 4D-Nucleofector System (Lonza Bioscience). After 48 hours, transfection efficiency was assessed in cells transfected with pmaxGFP (0.4 μg; Synthego) using fluorescence microscopy, and sgRNA/Cas9 transfected cells were plated in 96-well plates (one cell per well) for clonal expansion. Visual monitoring of single cell–derived clones was performed daily. The clones that were clearly derived from single cells were screened for BAG-1 protein levels by Western blot analysis and selected for study based on BAG-1 protein knockdown efficiency. Details of the BAG-1 sgRNAs used are listed in Supplementary Table S7. Cells transfected with Cas9 2NLS complexed with no sgRNA were used as control.

In vitro cell line proliferation

Cell proliferation was measured in parental, BAG-1 CRISPR KO or siRNA-treated prostate cancer cell lines in response to vehicle (0.1% DMSO) and Thio-2 (at various concentrations) using CellTiter-Glo (Promega) according to the manufacturer's instructions. Briefly, cells were plated in 96-well plates. For siRNA-treated cells, 24 hours after siRNA transfection, cells were seeded and subsequently (24 hours later) treated with either vehicle or Thio-2 in medium. For CRISPR clones and parental prostate cancer cell lines, siRNA transfection was omitted. CellTiter-Glo Luminescent Cell Viability Assay (Promega) or CyQUANT Cell Proliferation Assay (Thermo Fisher Scientific) were used to assay growth according to the manufacturer's instruction on day 0 or after 4 or 6 days of treatment and luminescence was measured using Synergy HTX (BioTek).

AR N-terminus and Thio-2 binding

Nuclear magnetic resonance (NMR) spectra were recorded at 278 K on either a Bruker 800 MHz Avance NEO or a 600 MHz Bruker Avance III spectrometer, equipped with TCl cryoprobes. Intensities and chemical shift perturbations (CSP) were obtained from $^{1}H,^{15}N$ correlation experiments and calculated using the following equation:

$$CSP = \sqrt{(\delta H)^2 - \left(\frac{\delta H}{5}\right)^2}$$

All spectra were referenced using sodium trimethylsilypropanesulfonate (DSS). NMR spectra were obtained for 25 μmol/L AR N-terminal domain (AR NTD) constructs $NTD_{1–518}$ and $NTD_{330–447}$ (Tau-5*) in the presence and absence of 250 μmol/L Thio2 and EPI-001. Samples were prepared in phosphate buffer [20 mmol/L sodium phosphate, pH 7.4, 1 mmol/L Tris (2-carboxy-ethyl)-phosphin-HCl (TCEP), 0.05% NaN_3], containing 10% D_2O, 10 μmol/L DSS and 0.5% DMSO-d_6. Experiments with ^{15}N-labeled AR NTD constructs $NTD_{1–518}$ and $NTD_{330–447}$ at 25 μmol/L were mixed with a 10 molar excess equivalents (250 μmol/L) of Thio-2 or EPI-001 (positive control) and measured at 5°C.

Plasmids

The plasmids used in this study were the pReceiver-M13 vector carrying a C-terminal fusion FLAG-tag (GeneCopoeia) containing either an empty cassette as control (CONTROL-FLAG) or the AR-FL (AR-FL-FLAG). An AR-V7 C-terminal fusion FLAG-tag (AR-V7-FLAG) was generated from the corresponding AR-FL-FLAG plasmid through restriction enzyme digest (XhoI, BSTE1I; New England Biosciences) and ligation techniques. The resulting plasmids were verified by sequencing (Beckman Coulter Genomics). The ARE3-PSA-luciferase (PSA-Luc) reporter plasmid has been described previously (48).

PSA luciferase reporter assay

PC3 cells were seeded at a density of 5,000 cells per well in 96-well plates in phenol-red free RPMI media supplemented with 10% charcoal-stripped FBS and concurrently transfected with either 0.5 μg/mL CONTROL-FLAG, AR-FL-FLAG or AR-V7-FLAG, and 0.25 μg/mL PSA-luc, using X-tremeGENE HP DNA Transfection Reagent (Merck) as per manufacturer's recommendations and incubated overnight. Cells were then treated with either vehicle (DMSO 0.1%), various concentrations (5, 10, or 50 μmol/L) of Thio-2 or 5 μmol/L enzalutamide for 1 hour prior to stimulation with or without 10 nmol/L DHT. Cells were then incubated for 16 hours and then lysed with Pierce IP Lysis Buffer (ThermoFisher Scientific). Luciferase Assay Reagent (Promega) was added to lysate and luciferase activity was measured using the BioTek Cytation 5 Cell Imaging Multimode Reader (Agilent).

Thio-2 solubility

Thio-2 solubility was measured by comparing Thio-2 aromatic signals (region 6.5–8 ppm) with DSS signal (internal reference, at 0 ppm) in 1D ^{1}H spectra. Samples containing variable concentrations of Thio-2 were prepared in NMR buffer, containing 10% D_2O, 10 μmol/L DSS and 0.5 or 2% DMSO-d_6. Samples were measured on 600 MHz spectrometer at 278, 298, and 310 K. Integration of Thio-2 ^{1}H aromatic signals (region 6.5–8 ppm) and the internal reference (DSS) ^{1}H signal (at 0 ppm) were used for quantification. Samples containing 5 μmol/L Thio-2, 10 μmol/L DSS, and variable amounts of DMSO-d_6 [buffer 20 mmol/L sodium phosphate (pH 7.4), 1 mmol/L TCEP, 10% D_2O, 0.05% NaN_3] were recorded on 600 MHz Bruker Avance spectrometer equipped with a cryoprobe.

Statistical analyses

Kruskal–Wallis test was used to determine the difference between ligandable properties of BAG-1, BCL2 and druggable protein kinase ATP site. Unpaired Student *t* tests were used to determine the

(*Continued.*) **C,** Mouse prostates from BAG-1 KO (red bars; $n = 5$) and BAG-1 WT (gray bars; $n = 6$) male mice at age 12 weeks were taken and samples prepared for RNA-seq. Median BAG isoforms and CHMP5 mRNA levels (fragments per kilobase of transcript per million reads; FPKM) with interquartile range, and smallest and largest value, is shown. *P* values were calculated for BAG-1 KO compared with BAG-1 WT mice using unpaired Student *t* test. *P* values ≤ 0.05 are shown. **D,** Overview of GSEA using MsigDB (v7.0) functional pathways: H, Hallmark; C2, Curated Gene Sets (including KEGG, Biocarta, Reactome). BAG-1 KO and BAG-1 WT RNA-seq analysis was compared, change in gene expression was ranked by $\log_2$ fold change, then tested for enrichment against functional gene sets (H, C2), using GSEA. The distribution of resulting FDR values ($\log_{10}$) is shown in red, and the threshold for significance (FDR 0.05) is shown by dotted grey line. None of the pathways tested reached the significance threshold. **E,** Kaplan–Meier curves of overall survival (OS) of BAG-1 KO (red line; $n = 9$) and BAG-1 WT (gray line; $n = 8$) male mice from birth. Median OS, HR with 95% confidence intervals and *P* values for univariate Cox survival model are shown. **F,** The body weight of male BAG-1 KO (red bars) and BAG-1 WT (gray bars) male mice at 12 weeks and 12 months was determined. Median body weight with interquartile range, and smallest and largest value, is shown. *P* values were calculated for BAG-1 KO compared with BAG-1 WT mice using unpaired Student *t* test. *P* values ≤ 0.05 are shown. **G,** The weight of the genitourinary tract, kidney, testis, prostate, and serum levels of testosterone, from male BAG-1 KO (red bar) and BAG-1 WT (gray bar) male mice at age 3 months and older was determined. Median weight or serum testosterone levels with interquartile range, and smallest and largest value, is shown. *P* values were calculated for BAG-1 KO compared with BAG-1 WT mice using unpaired Student *t* test. *P* values ≤ 0.05 are shown.

difference between mRNA expression of BAG-1 exon 2 deleted KO and WT mice. Overall survival of BAG-1 exon 2 deleted KO and WT mice were estimated using the Kaplan–Meier method, and respective hazard ratios (HRs) were obtained by Cox regression. Unpaired Student *t* tests were used to determine differences between characteristics of BAG-1 exon 2 deleted KO and WT mice. Unpaired Student *t* tests were used to determine differences between DHT stimulated genes in LNCaP shRNA clones. Unpaired Student *t* tests were used to determine differences in growth between LNCaP shRNA clones *in vitro* at day 27. Unpaired Student *t* tests were used to determine the difference between growth of PDX organoids (PDX-O), PDXs, and prostate cancer cell lines (with siRNA control/BAG-1 and CRISPR control/BAG-1) treated with vehicle or Thio-2. Unpaired Student *t* tests were used to determine the difference between mRNA expression of PDX-Os and prostate cancer cell lines (with siRNA control/BAG-1 and CRISPR control/BAG-1) treated with vehicle or Thio-2. Unpaired Student *t* tests were used to determine the difference between weights of non–tumor-bearing mice and organs treated with vehicle or Thio-2. The doubling time (2-fold growth) for CP50 PDXs were used as a surrogate endpoint for overall survival. Overall survival was estimated using the Kaplan–Meier method, and respective HRs were obtained by Cox regression. Unpaired Student *t* tests were used to determine the difference between serum PSA of PDXs treated with and without Thio-2. Bioinformatic analyses are detailed in associated sections. Statistical analyses were performed with GraphPad Prism Version 7 (GraphPad Software). All experimental replicates and statistical analyses performed are detailed in figure legends. Statistical significance was prespecified at $P \leq 0.05$. No adjustment for multiple testing has been made.

Study approvals

All patients treated at the RMH had provided written informed consent and were enrolled in institutional protocols approved by the Royal Marsden NHS Foundation Trust Hospital (London, United Kingdom) ethics review committee (reference 04/Q0801/60). All mouse work was carried out in accordance with the ICR guidelines, including approval by the ICR Animal Welfare and Ethical Review Body, and with the UK Animals (Scientific Procedures) Act 1986, and/or in accordance with the German national and KIT institutional guidelines, including approval by the KIT Animal Welfare and Ethical Review Body, and the Regierungspräsidium Karlsruhe, Germany.

Data availability statement

The cell line and mouse prostate RNA-seq data will be available under accession number PRJEB66442 from European Nucleotide Archive at time of publication.

Results

BAG-1 is highly expressed and associates with signaling pathways critical for the development and progression of CRPC

To investigate the importance of BAG-1 isoforms in CRPC, we interrogated the association between BAG-1 mRNA expression and the Molecular Signatures Database hallmark gene collection in two independent CRPC patient transcriptome cohorts (**Fig. 1A**; refs. 30–33). BAG-1 mRNA was highly expressed (top 25% expressed genes) in both CRPC transcriptome cohorts (**Fig. 1B** and **C**). Furthermore, BAG-1 mRNA expression positively correlated with multiple signaling pathways implicated in the development and progression of CRPC; including MYC targets V1 and V2, E2F targets, IL6 JAK STAT signaling, DNA repair, PI3K AKT MTOR signaling, MTORC1 signaling, and androgen response (**Fig. 1D** and **E**; refs. 30–32). Taken together, these data demonstrate that BAG-1 isoforms are highly expressed and associate with signaling pathways implicated in the development and progression of CRPC.

The BAG domain of the BAG-1 isoforms present a groove that provides a tractable but challenging drug target

Having demonstrated that BAG-1 isoform expression associates with critical signaling pathways in CRPC, we expanded our previous studies to investigate whether BAG-1 represents a tractable drug target (15). Therapies targeting the highly conserved BAG domain, present in all BAG-1 isoforms and critical for BAG-1 isoform function, provides an attractive strategy to abrogate BAG-1 activity in CRPC (8–10, 15–22). We had previously reported that the BAG domain of BAG-1 isoforms presents a groove, suitable for peptide or peptidomimetic modulators, but maybe challenging for small-molecule inhibition (15). Updated canSAR analysis demonstrates that the 44 3D HSC70-BAG domain structures continue to reveal a lack of a classical "ligandable" cavity within the BAG domain (**Fig. 2A**; Supplementary Table S1; refs. 15, 34, 35, 49, 50). We find that properties (except polar ratio) of the BAG domain groove fall outside the distributions expected for druggable cavities (all $P < 0.01$, Kruskal–Wallis test; **Fig. 2B**; refs. 15, 36, 51). We next wanted to explore whether a cryptic druggable cavity might emerge should we probe the structural fluctuations of the protein. To this end, we performed Monte Carlo simulations, which identified 4,489 cavities in 449 generated models (37). Despite allowances for structural fluctuations, the cavity of interest (80% of amino acid residues within the original pocket; 3FZLB) remains challenging for small-molecule inhibition (**Fig. 2C**). Furthermore, of the remaining cavities identified, only seven (of 4489) cavities have been identified as ligandable, and these may represent artifacts as they are only identified in a limited number of models (six of 449) derived (**Fig. 2C**). These updated analyses confirm that the BAG domain provides a tractable although challenging drug target with geometric and physicochemical properties that may require peptide or peptidomimetic approaches.

BAG-1 isoform KO impacts mouse hormone physiology suggesting that targeting the BAG domain should be associated with minimal "on-target" toxicity

BAG-1 is a multifunctional protein that binds numerous molecular targets to regulate a plethora of cellular processes (8–10). In light of this, one critical consideration is that therapies blocking BAG-1 function may be associated with modulation of normal physiology resulting in treatment-related adverse events. To further investigate this, we studied the impact of BAG-1 loss in BAG-1–deleted mouse models. Homozygous targeted deletion of exon 1 and 2 of the BAG-1 gene has previosuly been reported to be embryonically lethal (38). Analyzing these generated and previously reported BAG-1 heterozygous mice that are viable, we demonstrate that BAG-1 mRNA is indeed reduced but surprisingly CHMP5 (which is located on the opposite strand of chromosome 9 to BAG-1) is also downregulated in this model (Supplementary Fig. S1A; refs. 10, 52). CHMP5 deletion has been previously shown to be embryonically lethal and therefore may explain the phenotype previously reported for this BAG-1 KO model (52). Considering this, we explored an alternative KO strategy. We utilized a BAG-1 specific KO, first mouse strain Bag1tm1a (EUCOMM)Hmgu (referred to as BAG-1 KO from here on out), developed by the European Conditional Mouse Mutagenesis

(EUCOMM) Program to study the impact of losing just BAG-1 (**Fig. 3A**). These BAG-1 KO mice are viable and fertile, with BAG-1 deletion confirmed at the mRNA level, and following pan-mouse-BAG-1 antibody validation, at the protein level including in prostates isolated from KO mice and littermate controls (**Fig. 3A** and **B**; Supplementary Fig. S1B and S1C). In contrast to BAG-1 mRNA and protein levels, there was no change in protein expression or localization of the AR in prostates from BAG-1 KO mice when compared with WT mice (Supplementary Fig. S1C–S1E). To investigate the broader impact of BAG-1 deletion on gene expression and signaling pathways, RNA-seq was performed on BAG-1 KO and WT mouse prostates; this demonstrated significant ($P < 0.01$, Student t test) reductions in BAG-1 mRNA with no significant change in CHMP5 or other BAG family members (**Fig. 3C**). There was no significant enrichment in functional pathways in BAG-1 KO compared with WT mouse prostates (**Fig. 3D**). Consistent with this, BAG-1 deletion did not impact mouse overall survival (**Fig. 3E**; Supplementary Fig. S2A). The only characteristics that were different following BAG-1 deletion were decreased prostatic weight ($P = 0.05$, Student t test), increased duration of pregnancy ($P = 0.01$, Student t test), decreased litter size ($P = 0.04$, Student t test), increased day 1 neonatal weight ($P = 0.02$, Student t test), and decreased neonate survival rate on day 2 ($P = 0.04$, Student t test), potentially indicating a role for BAG-1 in hormone physiology phenotypically, although there was no obvious impact on AR levels or localization, and other signaling pathways, when interrogating mouse prostates specifically (**Fig. 3D**, **F**, and **G**; Supplementary Fig. S1C–S1E and S2B–S2D). In addition, histologic analysis of all major organs demonstrated no difference between BAG-1 KO and WT mice (Supplementary Fig. S3 and S4). These data suggest that therapies blocking the BAG-1 isoforms may impact hormone physiology phenotypically, which although it needs to be considered, should be associated with limited toxicity.

BAG-1 isoform knockdown induces a limited phenotype in the LNCaP cell line prostate cancer model

Considering the marked differences between BAG-1–associated signaling pathways in our patient correlative data and mouse KO studies, we explored the impact of BAG-1 knockdown in LNCaP shRNA clones (**Fig. 4A**). RNA-seq was performed on LNCaP control and BAG-1 shRNA clones; this demonstrated a significant ($P < 0.01$, Student t test) reduction in BAG-1 mRNA expression (**Fig. 4A**). There was de-enrichment in E2F targets and G_2–M checkpoint signatures that were both positively correlated with BAG-1 mRNA expression in our ICR/RMH CRPC transcriptome cohort (**Figs. 1E** and **4A**). However, there was no significant alternations in other functional pathways associated with BAG-1 mRNA expression in our patient CRPC transcriptome studies when comparing BAG-1 knockdown and control LNCaP shRNA clones (**Figs. 1D** and **E** and **4A**). Next, we explored the impact of BAG-1 isoform knockdown on specific AR-regulated genes (PSA, TMPRSS2, and FKBP5; **Fig. 4B**). BAG-1 knockdown significantly reduced DHT-mediated induction of FKBP5 ($P = 0.03$, Student t test) but had no significant impact on PSA and TMPRSS2 (**Fig. 4B**). Finally, we interrogated the impact of BAG-1 isoform knockdown on the growth of LNCaP cells *in-vivo*, demonstrating there was no significant difference in the growth of BAG-1 knockdown and control LNCaP shRNA clones (**Fig. 4C**). These data suggest that BAG-1 isoform knockdown induces a limited phenotype in this specific context and that targeting BAG-1 as a therapeutic target for lethal prostate cancer requires further interrogation.

Thio-2 inhibits the growth of CRPC patient-derived models with associated suppression of AR target genes

Despite the challenging geometric and physicochemical properties associated with targeting the BAG domain of BAG-1 isoforms and limited phenotype associated with BAG-1 isoform knockdown across

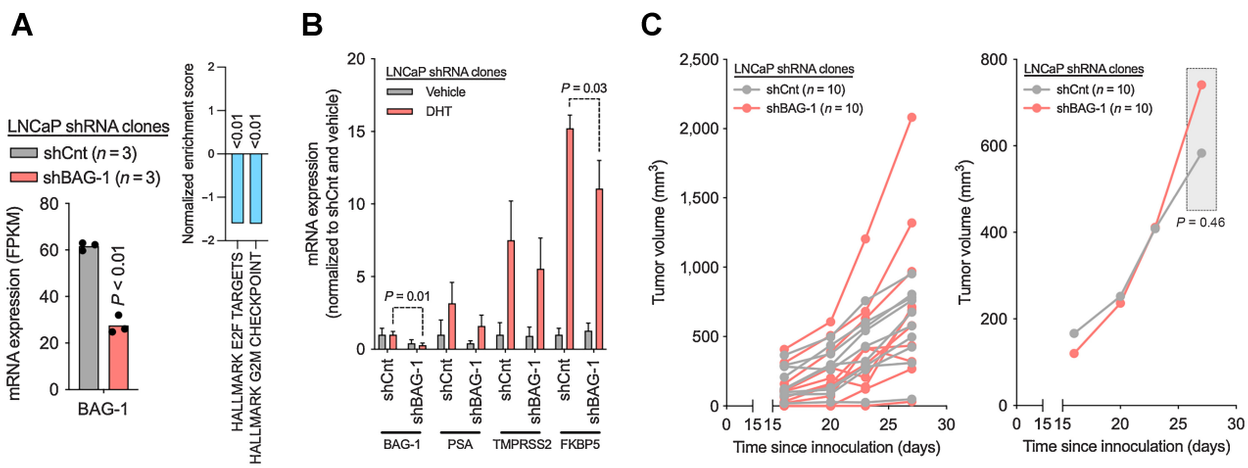

Figure 4.

BAG-1 isoform knockdown induces a limited phenotype in the LNCaP cell line prostate cancer model. **A,** LNCaP shRNA clones were collected and prepared for RNA-seq. Mean BAG-1 mRNA levels (FPKM) in control (gray bars; $n = 3$) and BAG-1 (red bars; $n = 3$) shRNA clones is shown. P values were calculated for BAG-1 shRNA (shBAG-1) clones compared with control shRNA (shCnt) clones using unpaired Student t test. P values ≤ 0.05 are shown. Analysis of RNA-seq with GESA shows BAG-1 knockdown associates with hallmark pathways. NESs and FDRs are shown. Hallmark pathways significantly (FDR ≤ 0.05) enriched and de-enriched with BAG-1 knockdown are shown. **B,** LNCaP shRNA clones were grown in starved media (10% charcoal-stripped serum) for 72 hours prior to treatment with vehicle (gray bars; Ethanol 0.1%) or 10 nmol/L DHT (red bars) for 16 hours and BAG-1, PSA, TMPRSS2 and FKBP5 mRNA expression was determined. Mean mRNA expression (normalized to average of GAPDH/B2M/HRPT1/RPLP0 and shCnt/vehicle; defined as 1) with SD from three individual experiments is shown. P values were calculated for the impact of BAG-1 knockdown on DHT stimulation using unpaired Student t test. P values ≤ 0.05 are shown. **C,** NSG male mice were inoculated with LNCaP shRNA control (shCnt; gray line; $n = 10$) or BAG-1 (shBAG-1; red line; $n = 10$) clones and growth was measured between days 16 and 27. Growth of all tumors (left) and mean growth (right) is shown. P values were calculated comparing shCnt and shBAG-1 at day 27 using unpaired Student t test.

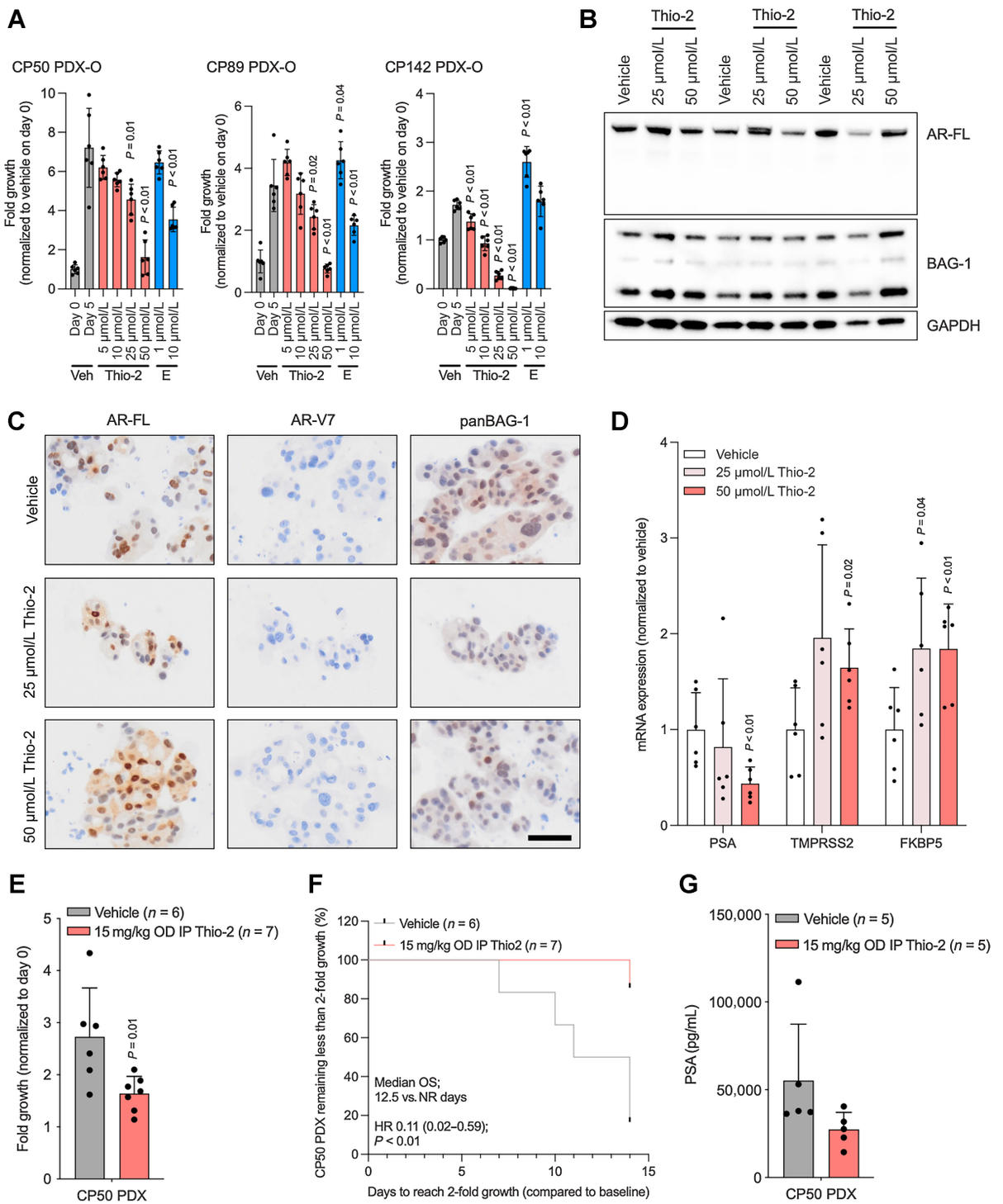

Figure 5.

Thio-2 inhibits the growth of CRPC patient-derived models with associated suppression of AR target genes. **A,** CP50, CP89, and CP142 PDX-Os were treated with vehicle (Veh, DMSO 0.1%), various concentrations (5, 10, 25, and 50 µmol/L) of Thio-2 or various concentrations (1 and 10 µmol/L) of enzalutamide (E), and growth determined after 5 days by CellTiter-Glo 3D Cell Viability Assay. Mean fold change in growth (compared with day 0) with SD from a single experiment with six replicates is shown. *P* values were calculated for each condition compared with vehicle at 5 days using unpaired Student *t* test. *P* values ≤ 0.05 are shown. **B,** CP50 PDX-O were treated with vehicle (DMSO 0.1%) or various concentrations (25 and 50 µmol/L) of Thio-2 for 17 hours. The effect of each condition on AR-FL, BAG-1, and GAPDH protein expression was determined. Single Western blot analysis with triplicates is shown. (*Continued on the following page.*)

a number of models, Thio-2 has been postulated to bind the BAG domain and block BAG-1 isoform function, including BAG-1L–mediated AR transactivation (15, 26, 53). We therefore explored the impact of Thio-2 on AR signaling and on the growth of patient-derived models of CRPC. We utilized three PDX models, CP50, CP89, and CP142, all of which were developed from lymph node biopsies of patients with CRPC (Supplementary Fig. S5A; refs. 54–56). PDX-Os were derived from these individual PDX models to support interrogation of Thio-2 *in vitro*. Having validated a panBAG-1 antibody for IHC, we demonstrated AR-FL, AR-V7, and BAG-1 isoform expression across all these PDXs and their related PDX-O models (Supplementary Fig. S5B and S5C). Thio-2 inhibited the growth of PDX-Os from CP50, CP89, and CP142 (**Fig. 5A**). Interestingly, enzalutamide maintained some growth inhibitory effects in CP50 and CP89, but not in CP142 (**Fig. 5A**). In the CP50 PDX-O model, Thio-2 appeared to have little impact on AR-FL and BAG-1 isoform protein expression although it suppressed PSA mRNA levels (at 50 μmol/L; **Fig. 5B**–**D**). In addition, AR-V7 protein was not detected in the CP50 PDX-O model *in vitro* (**Fig. 5B** and **C**). We next investigated Thio-2 *in vivo*, first exploring Thio-2 tolerability in non–tumor-bearing mice; we administered 15 mg/kg once daily intraperitoneally which significantly impacted heart weight ($P < 0.01$, Student *t* test), and reduced other parameters including kidney, testes, seminal vesicles, prostate, and body weight, although not significantly (Supplementary Fig. S6A–S6C). We next explored the impact of 15 mg/kg once daily intraperitoneally Thio-2 on AR signaling and growth in the tumor-bearing CP50 PDX, to determine whether any therapeutic impact was observed (Supplementary Fig. S6D). Thio-2 significantly ($P = 0.01$, Student *t* test) decreased tumor growth, and time to reach 2-fold tumor growth, of CP50 PDX compared with vehicle (**Fig. 5E** and **F**). In addition, Thio-2 treatment also reduced serum and tumor PSA protein levels (**Fig. 5G**; Supplementary Fig. S6E). Taken together, these *in vitro* and *in vivo* data demonstrate Thio-2 antitumor activity and pharmacodynamic modulation of AR signaling in patient-derived models of CRPC.

Thio-2 downregulates critical pathways, including AR signaling, implicated in prostate cancer development and progression

Following the interrogation of our patient-derived models, we explored the growth inhibitory effect of Thio-2 across multiple prostate cancer cell lines with varying levels of AR protein expression (**Fig. 6A**; Supplementary Fig. S6F). Although the AR-positive cell line LNCaP was most sensitive to Thio-2 treatment, both the growth of AR-positive (22Rv1) and AR-negative (DU145 and PC3) cell lines was inhibited at higher Thio-2 concentrations, suggesting not all Thio-2 growth inhibitory effects are mediated through AR-dependent mechanisms (**Fig. 6A**). To further explore this, RNA-seq was performed in LNCaP to investigate the broader effects of Thio-2 (50 μmol/L) on cellular pathways (**Fig. 6B**). Six pathways were found to be significantly enriched after Thio-2 treatment; Thio-2 treatment suppressed important pathways implicated in prostate cancer biology including androgen response [normalized enrichment score (NES) −2.43, FDR < 0.01], E2F targets (NES −2.96, FDR < 0.01), G_2–M checkpoints (NES −2.59, FDR < 0.01), MYC targets V1 (NES −2.38, FDR < 0.01), and MYC targets V2 (NES −2.14, FDR < 0.01; **Fig. 6C** and **D**). Next, we investigated whether lower concentrations (5 μmol/L) of Thio-2 are also sufficient to inhibit AR signaling and genome-wide AR binding in response to DHT (**Fig. 6E**). The expression of 471 genes significantly ($P \leq 0.05$, absolute $\log_2$ fold change > 1) changed in response to DHT (**Fig. 6F** and **G**). Treatment with 5 μmol/L Thio-2 led to a reduction in gene expression changes, with 151 (32%) of those 471 DHT-regulated genes remaining altered following DHT treatment (**Fig. 6F** and **H**). Furthermore, AR chromatin immunoprecipitation demonstrated a reduction in genome-wide AR binding (Supplementary Fig. S7). Overall, these data suggest that Thio-2 impacts critical pathways, including AR signaling, involved in the development and progression of CRPC.

The mechanism of action of Thio-2 is independent of BAG-1 isoform function

In light of Thio-2 being reported to inhibit BAG-1 isoform function, we next interrogated whether the observed mechanism of action of Thio-2 is dependent on the BAG-1 isoforms (15, 26, 53). BAG-1 isoform siRNA knockdown led to a small but significant increase in growth of LNCaP ($P = 0.02$, Student *t* test) and 22Rv1 ($P < 0.01$, Student *t* test), but not in LNCaP95 cells (**Fig. 7A**, **D**, and **G**). In addition, BAG-1 isoform siRNA knockdown had no effect on AR-FL, AR-V7, or PSA protein expression in all three cell lines (**Fig. 7B**, **E**, and **H**). Furthermore, BAG-1 isoform siRNA knockdown did not consistently suppress downstream AR target genes (**Fig. 7C**, **F**, and **I**). However, as previously shown, Thio-2 significantly inhibited the growth of LNCaP, 22Rv1, and LNCaP95 (**Figs. 6A**, **7A**, **D**, and **G**). This was irrespective of BAG-1 isoform siRNA knockdown status, suggesting that its growth inhibitory effects are not BAG-1 isoform mediated (**Fig. 7A**, **D**, and **G**). In contrast to BAG-1 knockdown, Thio-2 suppressed AR target genes more consistently across all cell lines tested, independent of BAG-1 isoform expression (**Fig. 7C**, **F**, and **I**). To further validate these findings, we developed 22Rv1 and LNCaP95 BAG-1 isoform CRISPR KO clones. BAG-1 isoform CRISPR KO using three different guides in 22Rv1 led to a significant (all $P < 0.01$, Student *t* test) increase in growth (Supplementary Fig. S8A). In contrast, BAG-1 isoform CRISPR KO using two different guides in LNCaP95 led to a significant ($P = 0.04$ and 0.03, Student *t* test) decrease in growth (Supplementary Fig. S8D). BAG-1 isoform CRISPR KO did not consistently impact AR-FL or AR-V7 protein levels in these cell lines (Supplementary Fig. S8B and S8E). In addition, BAG-1 isoform CRISPR KO did not significantly suppress any AR target genes, with

(*Continued.*) **C,** Representative micrographs of AR-FL, AR-V7, and pan BAG-1 (panBAG1) detection by IHC of formalin-fixed paraffin-embedded CP50 PDX-O treated with vehicle (DMSO 0.1%) or various concentrations (25 and 50 μmol/L) of Thio-2 for 17 hours are shown. Scale bar: 50 μm. **D,** CP50 PDX-O were treated with vehicle (DMSO 0.1%) or various concentrations (25 and 50 μmol/L) of Thio-2 for 17 hours. The effect of each condition on PSA, TMPRSS2 and FKBP5 mRNA expression was determined. Mean mRNA expression (normalized to average of GAPDH/B2M/HRPT1/RPLP0 and vehicle treatment; defined as 1) with SD from a single experiment with six replicates is shown. *P* values were calculated for each condition compared with vehicle using unpaired Student *t* test. *P* values ≤ 0.05 are shown. **E,** CP50 PDXs were treated with 15 mg/kg Thio-2 ($n = 7$) or vehicle ($n = 6$) once daily intraperitoneally for 14 days. Mean growth (normalized to day 0; defined as 1) with SD was determined on day 14. *P* values were calculated comparing 15 mg/kg Thio-2 IP OD treatment arm with vehicle control using unpaired Student *t* test. *P* values ≤ 0.05 are shown. **F,** The doubling time (2-fold growth) for CP50 PDXs were used as a surrogate endpoint for overall survival (OS). Median OS, HR with 95% confidence intervals and *P* values for univariate cox survival model are shown. **G,** The effect of 15 mg/kg Thio-2 OD IP compared with vehicle on serum PSA was determined at 5 days. Mean serum PSA with SD was determined for each mouse. *P* values were calculated for vehicle compared with 15 mg/kg Thio-2 once daily intraperitoneally using unpaired Student *t* test. *P* values ≤ 0.05 are shown.

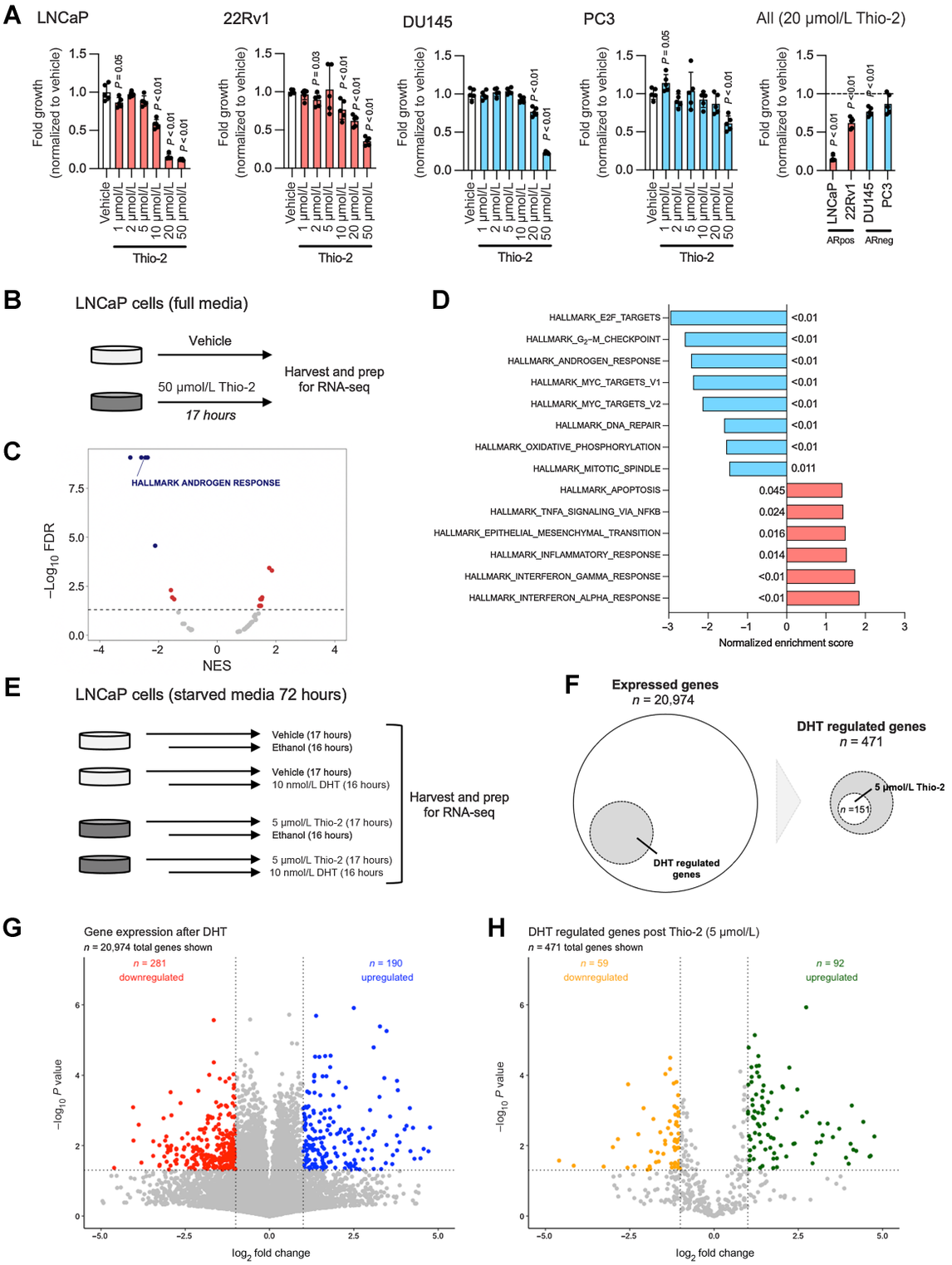

Figure 6.

Thio-2 downregulates critical pathways, including AR signaling, implicated in CRPC development and progression. **A,** AR-positive (LNCaP and 22Rv1) and AR-negative (DU145 and PC3) prostate cancer cells were treated with vehicle (DMSO 0.1%) or various concentrations (1, 2, 5, 10, 20, and 50 µmol/L) of Thio-2 and growth was determined after 4 days by CyQUANT Cell Proliferation Assay. Mean fold change in growth (compared with vehicle) with SD from a single experiment with five replicates is shown. *P* values were calculated for each condition compared with vehicle unpaired Student *t* test. *P* values ≤ 0.05 are shown. **B,** Schematic of RNA-seq experimental setup. LNCaP cells were grown in full media (10% FBS) prior to treatment with vehicle (DMSO 0.1%) or 50 µmol/L Thio-2 for 17 hours. RNA-seq was performed on a single experiment in triplicate. (*Continued on the following page.*)

several of them significantly increasing in response to BAG-1 KO (Supplementary Fig. S8C and S8F). Consistent with our siRNA studies, in our CRISPR models, Thio-2 treatment significantly inhibited the growth, and suppressed AR target gene expression more consistently, with this appearing to be independent of BAG-1 isoform expression (Supplementary Fig. S8A–S8F). Finally, as our RNA-seq data demonstrated that Thio-2 impacted other pathways including MYC targets V1 and V2, we explored the impact of Thio-2 treatment on C-MYC expression in our CP50 PDX-O and LNCaP95 BAG-1 isoform CRISPR KO clones (**Fig. 6D**; Supplementary Fig. S9A and S9B). Consistent with our RNA-seq analyses, Thio-2 treatment decreased C-MYC protein expression in both models, and this was independent of BAG-1 isoform function (Supplementary Fig. S9A and S9B). In addition, although Thio-2 treatment decreased C-MYC protein expression in LNCaP, LNCaP95, 22Rv1, and DU145 cell lines; C-MYC siRNA knockdown most consistently impacted the growth of DU145 cells, providing novel insights into the potential mechanism through which Thio-2 inhibits the growth of AR-negative cell lines (Supplementary Fig. S9C–S9F). Taken together, these studies confirm that Thio-2 inhibits AR signaling and decreases C-MYC expression to inhibit the growth of prostate cancer cell lines through a mechanism of action that, in these specific studies, appears to be independent of BAG-1 isoform function.

The mechanism of action of Thio-2 in prostate cancer models may be mediated, in part, through a novel interaction with the AR N-terminus

Having demonstrated that Thio-2 inhibits AR signaling and the growth of prostate cancer models independent of BAG-1 isoform function, we investigated whether its mechanism of action may be mediated through the AR NTD as it has previously been shown to inhibit AR NTD transactivation (15). EPI-001, which binds the AR NTD, leads to intensity changes in the NMR protein ^{1}H-^{15}N correlation spectra for the full-length AR NTD (residues 1–558) and chemical shift perturbations in the partially helical regions of a shorter transactivation unit 5 construct (residues 330–447; Supplementary Fig. S10A and S10B; refs. 57, 58). Although less intense, Thio-2 demonstrated changes in the same regions of AR, suggesting that it may bind the AR through by a similar binding mechanism (Supplementary Fig. S10C and S10D). Next, to further explore the impact on Thio-2 on AR transactivation, we interrogated the ability of Thio-2 to inhibit the transcriptional activity of both AR-FL and AR-V7. Thio-2 significantly inhibited the transactivation of the unstimulated and stimulated AR-FL, and the constitutively active AR-V7 (Supplementary Fig. S11). In contrast, enzalutamide only inhibited the stimulated AR-FL, further supporting that Thio-2 may function through the AR NTD, independent of BAG-1, and distinct from current inhibitors of the ligand-binding domain, such as enzalutamide (Supplementary Fig. S11). One important consideration is that Thio-2 does exhibit limited solubility, and although low micromolar concentrations at which growth inhibition and AR signaling suppression are observed can be achieved, those phenotypes seen at much higher concentrations should be interpreted with caution (Supplementary Fig. S12). These studies suggest that the mechanism of action of Thio-2, and the associated phenotype observed, may be mediated, in part, through a novel interaction with the AR NTD, although other mechanisms of action are also likely and require further elucidation. These data support the interrogation of related compounds with improved drug-like properties, that elicit the same phenotype, as a novel therapeutic strategy for CRPC.

Discussion

The clinical relevance of BAG-1 isoforms in prostate cancer has been studied extensively by IHC. These studies have demonstrated increased BAG-1L protein expression as castration resistance develops (24, 25). In addition, multiple studies have demonstrated nuclear BAG-1 protein expression to associate with clinical benefit from AR-targeting therapies, and cytoplasmic BAG-1 protein expression to associate with benefit from radiotherapy in localized disease (15, 24, 25). To expand on these data and overcome the challenges associated with preanalytic variables, we explored BAG-1 mRNA isoform expression and its associations with signaling pathways in two independent CRPC patient transcriptome cohorts (30–32, 59, 60). BAG-1 mRNA was highly expressed and associated with key pathways, such as MYC targets V1 and V2, E2F targets, IL6 JAK STAT signaling, DNA repair, PI3K AKT MTOR signaling, MTORC1 signaling, and androgen response, that have been linked to the development and progression of CRPC (3, 61–64). Interestingly, BAG-1 mRNA isoform expression was only associated with androgen response in the SU2C/PCF cohort, which may, in part, be due to the fact that only around half of these patients had received an AR-targeting therapy compared with all of the patients in the ICR/RMH cohort (30–32). In addition, our mechanistic studies point to the fact that BAG-1 isoforms may not play a critical role in activation of the unstimulated AR, and this also needs to be considered. These findings are consistent with BAG-1 isoforms being multifunctional proteins that interact with a wide range of molecular targets to modulate multiple cellular processes supporting the development and progression of CRPC (8–10).

Critically, expansion of our previous druggability analyses demonstrate the BAG domain of BAG-1 isoforms to present a groove with geometric and physicochemical properties consistent with drug tractability that may be most suited to peptide or peptidomimetic approaches as opposed to traditional small molecule inhibition. One concern with therapeutic inhibition of a multifunctional protein that regulates a plethora of physiologic processes is "on-target" toxicity (8–10). However, in contrast to previous studies that demonstrated BAG-1 homozygous KO to be embryonically lethal, our

(*Continued.*) **C,** Analysis of RNA-seq with GESA shows Thio-2 treatment associates with hallmark pathways. NESs and FDRs are shown. Dotted line indicates significant threshold (FDR 0.05). Colored dots denote significant Hallmark pathways enriched and de-enriched with Thio-2 treatment. **D,** Hallmark pathways significantly (FDR ≤ 0.05) enriched and de-enriched with Thio-2 treatment are shown. **E,** Schematic of RNA-seq experimental setup. LNCaP cells were grown in starved media (10% charcoal-stripped serum) for 72 hours prior to treatment with vehicle (DMSO 0.1%) or 5 μmol/L Thio-2. Following 1 hour pretreatment with vehicle or 5 μmol/L Thio-2; cells were treated with vehicle (Ethanol 0.1%) or 10 nmol/L DHT for 16 hours (17 hours total treatment). RNA-seq was performed on a single experiment in triplicate. **F–H,** DHT regulated genes ($n = 471$) were identified by quantifying mRNA expression in starved (vehicle; Ethanol 0.1%) media and DHT induced media (P value ≤ 0.05, absolute $\log_2$ fold change > 1; **F**, **G**). Out of 471 DHT regulated genes, 151 remain differentially expressed after Thio-2 treatment at 5 μmol/L (**F**, **H**). Venn and volcano plots are shown. Horizontal dotted line indicates the significance threshold ($P = 0.05$). Vertical dotted line indicates the fold change threshold (absolute $\log_2$ fold change > 1).

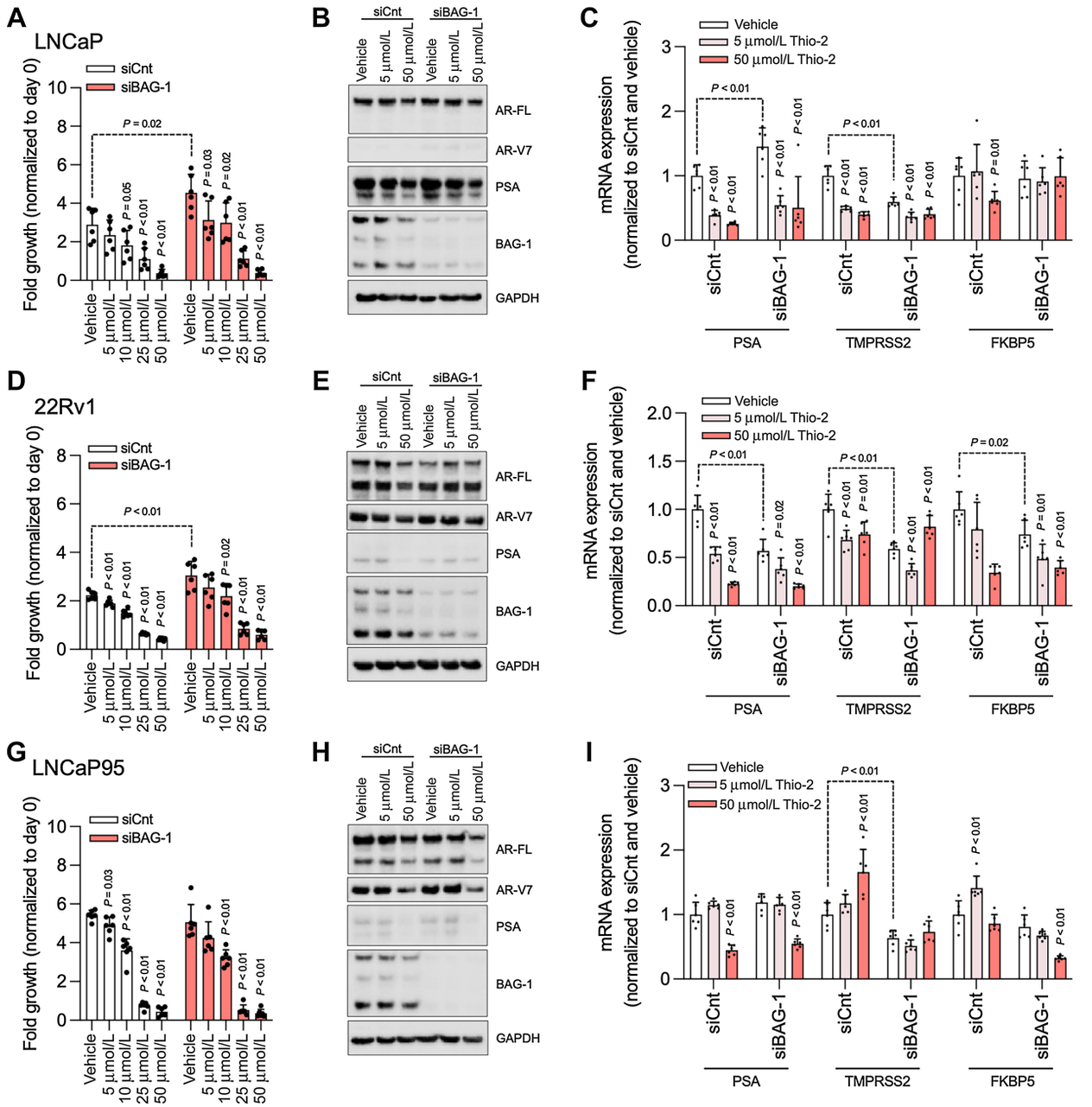

Figure 7.

Thio-2 downregulates androgen receptor signaling and inhibits growth of prostate cancer cell lines through a BAG-1–independent mechanism. LNCaP (**A**), 22Rv1 (**D**), and LNCaP95 (**G**) prostate cancer cells were transfected with 50 nmol/L of either control (siCnt; clear bars) or BAG-1 (siBAG-1; red bars) siRNA for 72 hours prior to treatment with vehicle (DMSO 0.1%) or various concentrations (5, 10, 25, and 50 µmol/L) of Thio-2 and growth was determined after 6 days by CellTiter-Glo Luminescent Cell Viability Assay. Mean fold change in growth (compared with day 0) with SD from a single experiment with six replicates is shown. *P* values were calculated for each condition compared with vehicle in siCnt and siBAG-1 cells, and between vehicle-treated siCnt and siBAG-1 cells (dotted lines), using unpaired Student *t* test. *P* values ≤ 0.05 are shown. LNCaP (**B**) 22Rv1 (**E**), and LNCaP95 (**H**) prostate cancer cells were transfected with 50 nmol/L of either siCnt or siBAG-1 siRNA for 55 hours prior to treatment with vehicle (DMSO 0.1%) or various concentrations (5 and 50 µmol/L) of Thio-2 for 17 hours (total 72 hours) and AR-FL, AR-V7, PSA, BAG-1, and GAPDH protein expression was determined. Single Western blot analysis is shown. LNCaP (**C**), 22Rv1 (**F**), and LNCaP95 (**I**) prostate cancer cells were transfected with 50 nmol/L of either siCnt or siBAG-1 siRNA for 55 hours prior to treatment with vehicle (DMSO 0.1%) or various concentrations (5 and 50 µmol/L) of Thio-2 for 17 hours (total 72 hours) and PSA, TMPRSS2, and FKBP5 mRNA expression was determined. Mean mRNA expression (normalized to average of GAPDH/B2M/HRPT1/RPLP0 and siCnt/vehicle; defined as 1) with SD from a single experiment with six replicates is shown. *P* values were calculated for each condition compared with vehicle in siCnt and siBAG-1 cells, and between vehicle-treated siCnt and siBAG-1 cells (dotted lines), using unpaired Student *t* test. *P* values ≤ 0.05 are shown.

alternative strategy identified BAG-1 KO mice to be viable and fertile (15, 38). Interestingly, male mice had smaller prostates, and pregnant female mice had increased duration of pregnancy, decreased litter size, increased neonatal weight on day 1 and decreased neonatal survival on day 2, which may point to the known role of BAG-1 isoforms in hormone physiology (15, 17–19). However, it is important to note, that although this phenotype was observed, analyses of AR levels or localization, and signaling pathways, specifically in the mouse prostates identified no obvious underpinning mechanism. The difference in the phenotype observed when compared with previous studies may be a consequence of BAG-1 being located close to CHMP5 (opposite strand of chromosome 9), and the apparent down regulation of both genes, with CHMP5 being responsible for the phenotype observed (38, 52). A further consideration is that our strategy results in a small portion of the BAG-1 N-terminus being expressed that may confer functionality, as although C-terminal BAG domain mediated protein–protein interactions are reported to be critical for BAG-1 isoform function, the N-terminus of BAG-1L has been shown to play a role in regulating the AR (8–10, 15–23). Finally, our observations are consistent with the development of BAG-1 KO embryonic stem cells that maintained pluripotency and the ability to differentiate, and studies of cancer cell lines where BAG-1 is rarely essential for cell survival (53, 65, 66).

A further consideration is that although BAG-1 mRNA associates with key signaling pathways implicated in the development and progression of prostate cancer in CRPC patient transcriptomes; this was not recapitulated in RNA-seq analyses of normal mouse prostates and LNCaP cells with BAG-1 KO/knockdown, and no significant phenotype was observed with BAG-1 KO/knockdown across multiple prostate cancer cell lines (3, 61–64). This is an important observation, as although one could postulate that BAG-1 function may be critical in the context of human disease complexity, which is very different to normal mouse prostate development and *in vitro/vivo* prostate cancer cell line models, or BAG-1 KO/knockdown may be incomplete, it also suggests that BAG-1 function may not be critical for prostate cancer cell survival and this requires careful consideration if targeting BAG-1 is to be pursued as a therapeutic target for this common disease.

Thio-2, a novel compound derived from Thioflavin S, has been predicted to bind the BAG domain of BAG-1 isoforms though *in silico* docking experiments, and studies in melanoma, breast and prostate cancer cell lines, have suggested a reduction in binding of BAG-1 to its binding partners (such as HSC/P70, BRAF, and AR), to inhibit AR, MEK, and AKT signaling (15, 26, 53). Intriguingly, Thio-2 inhibits AR signaling, and other important pathways, such as E2F targets, G_2–M checkpoints, MYC targets V1 and MYC targets V2, implicated in the development and progression of CRPC, to inhibit the growth of treatment-resistant prostate cancer cell lines and patient-derived prostate cancer models. It is therefore unsurprising that, although LNCaP cells which are AR-positive were the most sensitive to Thio-2 treatment, higher concentrations of Thio-2 inhibited the growth of AR-negative cell lines, as this is likely mediated through AR-independent molecular mechanisms. This was further supported by the demonstration that, although Thio-2 decreased C-MYC protein expression in multiple prostate cancer models, AR-negative cell lines were more sensitive to C-MYC protein knockdown, suggesting Thio-2 may inhibit the growth of AR-negative cell lines through a C-MYC–mediated mechanism.

Interestingly, enzalutamide maintained some growth inhibitory effects across two PDX-O models (CP50 and CP89) tested while Thio-2 demonstrated activity across all three PDX-O tested. Although these PDX models were developed from metastatic lymph node biopsies of patients with CRPC, we have previously demonstrated that AR-V7 protein expression, a common mechanism of resistance to AR-directed therapies, increases in response to castration and is suppressed by testosterone (55, 56). Consistent with this, our PDX models (CP50, CP89 and CP142; maintained in intact mice) have no/low levels of AR-V7 protein expression, and when grown as PDX-Os *in vitro* demonstrate no measurable AR-V7 protein expression. This raises the possibility of resensitization to therapies targeting the AR which will be important to further understand mechanistically, especially in the context of ongoing studies exploring bipolar androgen therapy as a therapeutic approach in CRPC (67).

Importantly, neither our BAG-1 isoform knockdown or KO studies recapitulated or rescued the Thio-2 phenotype observed, suggesting that the mechanism of action of Thio-2 is independent of BAG-1 function, in those specific molecular backgrounds studied. Interestingly, siRNA-mediated BAG-1 isoform knockdown increased growth in LNCaP and 22Rv1 cells, but not LNCaP95 cells. Furthermore, CRISPR mediated BAG-1 isoform KO increased growth in 22Rv1 cells but decreased growth in LNCaP95 cells. Although BAG-1 isoform knockdown or KO had limited consistent antitumor efficacy in the CRPC models studied, it is important to note that this may be context dependent. In addition, the generation of CRISPR mediated BAG-1 isoform KO clones from heterogenous cell populations, such as LNCaP95, may explain some of the differential effects seen between knockdown and KO approaches (68). It will be important to consider these results and the implications for targeting BAG-1 isoforms in prostate and other cancers. It will be critical to further understand the role of BAG-1 isoforms in the context of the activated AR in CSPC, different molecular backgrounds, and different diseases, to fully determine whether BAG-1 isoform targeting should be pursued for anticancer drug discovery efforts (15, 17, 18). This is further emphasized by studies in multiple breast cancer cell lines that have demonstrated differential response in growth to BAG-1 knockdown or KO (53, 69).

Consistent with these findings, we identified that Thio-2 may bind directly to the AR NTD through a similar mechanism to that of EPI-001, blocking both AR-FL and AR-V7 transactivation in reporter-based assays, suggesting, in part, a novel mechanism of Thio-2 action in CRPC (58). This may not be unexpected as cell-based assays investigating the impact of BAG-1L on AR transactivation have commonly utilized the AR NTD (15, 18). However, one consideration is that Thio-2 does exhibit limited solubility, and although low micromolar concentrations at which growth inhibition and AR signaling suppression can be achieved, one should exercise caution when interpreting those phenotypes observed at much higher concentrations, and when considering the *in vivo* analyses as both systemic and tumor Thio-2 concentrations were not determined. Furthermore, treatment with Thio-2 led to a reduction in heart weight *in vivo*, and although no other significant sequelae were identified, treatment was relatively short-term, and this would need to be considered if more drug-like compounds were to be pursued. Importantly, the attractive phenotype exhibited supports the development of similar, more drug-like compounds, such as A4B17 and X15695, as a novel therapeutic approach for CRPC (27–29). However, it will be important to understand whether these compounds share a similar mechanism of action and elicit the same phenotype in CRPC models (27, 28). Importantly, although the AR NTD remains a

challenging drug target, these data highlight the clinical potential of therapies targeting the AR NTD which are currently undergoing clinical evaluation in CRPC (70, 71).

In summary, we demonstrate the clinical relevance of BAG-1 isoform expression in CRPC and identify BAG-1 isoforms to be tractable but challenging drug target with KO mouse models supporting the tolerability of blocking BAG-1 function therapeutically. Despite these promising data, genomic abrogation of BAG-1 isoforms appeared to have limited antitumor efficacy in the CRPC models studied suggesting protein redundancy. Importantly, although probably independent of BAG-1 isoform function, Thio-2 suppressed AR signaling and other key prostate cancer signaling pathways to inhibit the growth of CRPC models. This observed phenotype appeared to be, at least in part, mediated through direct binding to the AR NTD. These data support further development of similar, more drug-like compounds, such as A4B17 and X15695, as novel therapeutics for CRPC, and highlight the clinical potential of treatments that block persistent AR signaling which are currently undergoing clinical evaluation in CRPC (27–29, 70, 71).

Authors' Disclosures

L. Cato reports grants from Claudia Adams Barr and Prostate Cancer Foundation during the conduct of the study; non-financial support from Sanofi outside the submitted work. I.I. Lee reports grants from Department of Defense during the conduct of the study; personal fees from Abbvie outside the submitted work. X. Salvatella reports grants and personal fees from Nuage Therapeutics outside the submitted work; in addition, X. Salvatella has a patent for EP21382254 pending and licensed to Nuage Therapeutics, a patent for EP22382068 pending and licensed to Nuage Therapeutics, and a patent for PCTEP2021076120 pending; and X. Salvatella is co-founder and consultant of Nuage Therapeutics. B. Al-Lazikani reports grants from Cancer Research UK and Cancer Prevention and Research Institute of Texas during the conduct of the study. M. Brown reports other support from Dana-Farber Cancer Institute and Harvard Medical School during the conduct of the study; grants from Novartis, personal fees from Novartis; personal fees and other support from Kronos Bio and GV20 Therapeutics outside the submitted work. A.C.B. Cato reports grants from Prostate Cancer Foundation during the conduct of the study. J.S. de Bono reports personal fees from AstraZeneca, Bioxcel Therapeutics, Boehringer Ingelheim, ImCheck Therapeutics, Qiagen, Terumo; grants and personal fees from Astellas, Amgen, Bayer, Cellcentric, Crescendo, Daiichi, Genentech/Roche, Genmab, Harpoon, Janssen, Merck Serono, Merck Sharp & Dohme, Menarini/Silicon Biosystems, MetaCurUm, Myricx, Nurix Therapeutics, Oncternal, Orion, Sanofi Aventis, Sierra Oncology, Taiho, and Vertex Pharmaceuticals; other support from Dark Blue Therapeutics, Eisai Therapeutics, GSK, Takeda, Tango Therapeutics; grants from Immunic Therapeutics; personal fees and other support from Novartis; grants and other support from Pfizer outside the submitted work; in addition, J.S. de Bono has a patent for DNA Damage repair inhibitors for treatment of Cancer licensed to AstraZeneca and a patent for 17-substituted steroids useful in cancer treatment licensed to Janssen. A. Sharp is an employee of the ICR, which has a commercial interest in abiraterone, PARP inhibition in DNA repair defective cancers, and PI3K/AKT pathway inhibitors (no personal income). A. Sharp has received travel support from Sanofi, Roche-Genentech and Nurix, and speaker honoraria from Astellas Pharma and Merck Sharp & Dohme. A. Sharp has served as an advisor to DE Shaw Research, CHARM Therapeutics, Ellipses Pharma and Droia Ventures. A. Sharp has been the CI/PI of industry-sponsored clinical trials. No disclosures were reported by the other authors.

Authors' Contributions

A. Neeb: Conceptualization, data curation, formal analysis, validation, investigation, visualization, methodology, writing–original draft, writing–review and editing. **I. Figueiredo:** Data curation, formal analysis, validation, investigation, visualization, methodology, writing–original draft, writing–review and editing. **D. Bogdan:** Data curation, formal analysis, validation, investigation, visualization, methodology, writing–original draft, writing–review and editing. **L. Cato:** Conceptualization, data curation, formal analysis, funding acquisition, validation, investigation, visualization, methodology, writing–review and editing. **J. Stober:** Data curation, formal analysis, validation, investigation, visualization, methodology, writing–review and editing. **J.M. Jiménez-Vacas:** Data curation, formal analysis, validation, investigation, visualization, methodology, writing–original draft, writing–review and editing. **V. Gourain:** Data curation, formal analysis, validation, investigation, visualization, methodology, writing–original draft, writing–review and editing. **I.I. Lee:** Data curation, formal analysis, validation, investigation, visualization, methodology. **R. Seeger:** Data curation, formal analysis, validation, investigation, visualization, methodology. **C. Muhle-Goll:** Data curation, formal analysis, validation, investigation, visualization, methodology. **B. Gurel:** Data curation, formal analysis, validation, investigation, visualization, methodology. **J. Welti:** Data curation, formal analysis, validation, investigation, visualization, methodology, writing–original draft. **D. Nava Rodrigues:** Data curation, formal analysis, validation, investigation, visualization, methodology. **J. Rekowski:** Data curation, formal analysis, methodology, writing–original draft, writing–review and editing. **X. Qiu:** Data curation, supervision, investigation, visualization, methodology. **Y. Jiang:** Data curation, supervision, investigation, visualization, methodology. **P. Di Micco:** Data curation, formal analysis, validation, investigation, visualization, methodology, writing–original draft. **B. Mateos:** Data curation, formal analysis, validation, investigation, visualization, methodology, writing–original draft, writing–review and editing. **S. Bielskutė:** Data curation, formal analysis, validation, investigation, visualization, methodology, writing–original draft, writing–review and editing. **R. Riisnaes:** Data curation, formal analysis, validation, investigation, visualization, methodology, writing–review and editing. **A. Ferreira:** Data curation, formal analysis, validation, investigation, visualization, methodology, writing–review and editing. **S. Miranda:** Data curation, formal analysis, validation, investigation, visualization, methodology, writing–review and editing. **M. Crespo:** Data curation, formal analysis, validation, investigation, visualization, methodology, writing–review and editing. **L. Buroni:** Data curation, formal analysis, validation, investigation, visualization, methodology. **J. Ning:** Data curation, formal analysis, validation, investigation, visualization, methodology. **S. Carreira:** Data curation, formal analysis, supervision, validation, investigation, visualization, methodology, writing–review and editing. **S. Bräse:** Resources, supervision, funding acquisition, writing–review and editing. **N. Jung:** Resources, supervision, funding acquisition, writing–review and editing. **S. Gräßle:** Resources, supervision, writing–original draft, writing–review and editing. **A. Swain:** Conceptualization, data curation, formal analysis, supervision, validation, investigation, visualization, methodology, writing–original draft. **X. Salvatella:** Conceptualization, resources, formal analysis, supervision, validation, investigation, visualization, methodology, writing–original draft, writing–review and editing. **S.R. Plymate:** Conceptualization, resources, supervision, funding acquisition, writing–original draft, writing–review and editing. **B. Al-Lazikani:** Conceptualization, resources, data curation, software, formal analysis, supervision, funding acquisition, validation, investigation, visualization, methodology, writing–original draft, writing–review and editing. **H.W. Long:** Data curation, formal analysis, supervision, validation, investigation, visualization, methodology, writing–original draft. **W. Yuan:** Data curation, supervision, validation, investigation, visualization, methodology, writing–original draft, writing–review and editing. **M. Brown:** Resources, supervision, funding acquisition. **A.C.B. Cato:** Conceptualization, resources, data curation, supervision, funding acquisition, writing–original draft, writing–review and editing. **J.S. de Bono:** Conceptualization, resources, supervision, funding acquisition, writing–original draft, writing–review and editing. **A. Sharp:** Conceptualization, resources, data curation, formal analysis, supervision, funding acquisition, investigation, visualization, methodology, writing–original draft, writing–review and editing.

Acknowledgments

The authors gratefully acknowledge the patients and the families of patients who contributed to this study. This work was supported by the Claudia Adam Barr Foundation (Funding to L. Cato), Prostate Cancer UK (Travelling Prize Fellowship to J.M. Jiménez-Vacas; Research Funding to J.S. de Bono and A. Sharp), the Asociación Española contra el Cáncer (Funding to B. Mateos), MINECO (Grants BIO2015-70092-R and PID2019-110198RB-I00 to X. Salvatella), Medical Research Council (Clinical Research Training Fellowship to A. Sharp; Research Funding to J.S. de Bono), The Academy of Medical Sciences (Starter Grant for Clinical Lecturers to A. Sharp), the Prostate Cancer Foundation (Young Investigator Awards to L. Cato, A. Sharp; Challenge Awards to L. Cato, S.R. Plymate, M. Brown, A.C.B. Cato, J.S. de Bono, and A. Sharp), Cancer Prevention and Research Institute of Texas (Funding to B. Al-Lazikani), the Movember Foundation through the London Movember Centre of Excellence (CEO13 2-002 to J.S. de Bono), the Wellcome Trust (Clinical Research Career Development Fellowship to A. Sharp), the National Institute for Health and Care Research Biomedical Research Centre

(Funding to A. Sharp), the Veterans Affairs Research and Development Service (to S.R. Plymate), and Cancer Research UK (Drug Discovery Committee Strategic Award to B. Al-Lazikani; Centre Programme and Experimental Cancer Medicine Centre grants to J.S. de Bono). J.S. de Bono is a National Institute for Health Research (NIHR) Senior Investigator. The views expressed in this article are those of the author(s) and not necessarily those of the National Health Service, the NIHR, or the Department of Health.

Note

Supplementary data for this article are available at Molecular Cancer Therapeutics Online (http://mct.aacrjournals.org/).

Received June 8, 2023; revised September 26, 2023; accepted February 22, 2024; published first February 27, 2024.

References

1. Siegel RL, Miller KD, Jemal A. Cancer statistics, 2020. CA Cancer J Clin 2020;70:7–30.
2. Sartor O, de Bono JS. Metastatic prostate cancer. N Engl J Med 2018;378:1653–4.
3. Westaby D, Fenor de La Maza MLD, Paschalis A, Jimenez-Vacas JM, Welti J, de Bono J, et al. A new old target: androgen receptor signaling and advanced prostate cancer. Annu Rev Pharmacol Toxicol 2022;62:131–53.
4. Armstrong AJ, Halabi S, Luo J, Nanus DM, Giannakakou P, Szmulewitz RZ, et al. Prospective multicenter validation of androgen receptor splice variant 7 and hormone therapy resistance in high-risk castration-resistant prostate cancer: the PROPHECY study. J Clin Oncol 2019;37:1120–9.
5. Sharp A, Coleman I, Yuan W, Sprenger C, Dolling D, Rodrigues DN, et al. Androgen receptor splice variant-7 expression emerges with castration resistance in prostate cancer. J Clin Invest 2019;129:192–208.
6. Annala M, Vandekerkhove G, Khalaf D, Taavitsainen S, Beja K, Warner EW, et al. Circulating tumor DNA genomics correlate with resistance to abiraterone and enzalutamide in prostate cancer. Cancer Discov 2018;8:444–57.
7. Romanel A, Gasi Tandefelt D, Conteduca V, Jayaram A, Casiraghi N, Wetterskog D, et al. Plasma AR and abiraterone-resistant prostate cancer. Sci Transl Med 2015;7:312re10.
8. Townsend PA, Cutress RI, Sharp A, Brimmell M, Packham G. BAG-1: a multifunctional regulator of cell growth and survival. Biochim Biophys Acta 2003;1603:83–98.
9. Sharp A, Crabb SJ, Townsend PA, Cutress RI, Brimmell M, Wang XH, et al. BAG-1 in carcinogenesis. Expert Rev Mol Med 2004;6:1–15.
10. Lee II, Kuznik NC, Rottenberg JT, Brown M, Cato ACB. BAG1L: a promising therapeutic target for androgen receptor-dependent prostate cancer. J Mol Endocrinol 2019;62:R289–R99.
11. Packham G, Brimmell M, Cleveland JL. Mammalian cells express two differently localized Bag-1 isoforms generated by alternative translation initiation. Biochem J 1997;328:807–13.
12. Briknarova K, Takayama S, Brive L, Havert ML, Knee DA, Velasco J, et al. Structural analysis of BAG1 cochaperone and its interactions with Hsc70 heat shock protein. Nat Struct Biol 2001;8:349–52.
13. Sondermann H, Scheufler C, Schneider C, Hohfeld J, Hartl FU, Moarefi I. Structure of a Bag/Hsc70 complex: convergent functional evolution of Hsp70 nucleotide exchange factors. Science 2001;291:1553–7.
14. Takayama S, Xie Z, Reed JC. An evolutionarily conserved family of Hsp70/Hsc70 molecular chaperone regulators. J Biol Chem 1999;274:781–6.
15. Cato L, Neeb A, Sharp A, Buzon V, Ficarro SB, Yang L, et al. Development of Bag-1L as a therapeutic target in androgen receptor-dependent prostate cancer. eLife 2017;6:e27159.
16. Froesch BA, Takayama S, Reed JC. BAG-1L protein enhances androgen receptor function. J Biol Chem 1998;273:11660–6.
17. Knee DA, Froesch BA, Nuber U, Takayama S, Reed JC. Structure-function analysis of Bag1 proteins. Effects on androgen receptor transcriptional activity. J Biol Chem 2001;276:12718–24.
18. Shatkina L, Mink S, Rogatsch H, Klocker H, Langer G, Nestl A, et al. The cochaperone Bag-1L enhances androgen receptor action via interaction with the NH2-terminal region of the receptor. Mol Cell Biol 2003;23:7189–97.
19. Cutress RI, Townsend PA, Sharp A, Maison A, Wood L, Lee R, et al. The nuclear BAG-1 isoform, BAG-1L, enhances oestrogen-dependent transcription. Oncogene 2003;22:4973–82.
20. Townsend PA, Cutress RI, Sharp A, Brimmell M, Packham G. BAG-1 prevents stress-induced long-term growth inhibition in breast cancer cells via a chaperone-dependent pathway. Cancer Res 2003;63:4150–7.
21. Sharp A, Crabb SJ, Johnson PW, Hague A, Cutress R, Townsend PA, et al. Thioflavin S (NSC71948) interferes with Bcl-2-associated athanogene (BAG-1)-mediated protein-protein interactions. J Pharmacol Exp Ther 2009;331:680–9.
22. Sharp A, Cutress RI, Johnson PW, Packham G, Townsend PA. Short peptides derived from the BAG-1 C-terminus inhibit the interaction between BAG-1 and HSC70 and decrease breast cancer cell growth. FEBS Lett 2009;583:3405–11.
23. Jehle K, Cato L, Neeb A, Muhle-Goll C, Jung N, Smith EW, et al. Coregulator control of androgen receptor action by a novel nuclear receptor-binding motif. J Biol Chem 2014;289:8839–51.
24. Krajewska M, Turner BC, Shabaik A, Krajewski S, Reed JC. Expression of BAG-1 protein correlates with aggressive behavior of prostate cancers. Prostate 2006;66:801–10.
25. Maki HE, Saramaki OR, Shatkina L, Martikainen PM, Tammela TL, van Weerden WM, et al. Overexpression and gene amplification of BAG-1L in hormone-refractory prostate cancer. J Pathol 2007;212:395–401.
26. Enthammer M, Papadakis ES, Salome Gachet M, Deutsch M, Schwaiger S, Koziel K, et al. Isolation of a novel thioflavin S-derived compound that inhibits BAG-1-mediated protein interactions and targets BRAF inhibitor-resistant cell lines. Mol Cancer Ther 2013;12:2400–14.
27. Kuznik NC, Solozobova V, Jung N, Grassle S, Lei Q, Lewandowski EM, et al. Development of a benzothiazole scaffold-based androgen receptor N-terminal inhibitor for treating androgen-responsive prostate cancer. ACS Chem Biol 2021;16:2103–8.
28. Kuznik NC, Solozobova V, Lee II, Jung N, Yang L, Nienhaus K, et al. A chemical probe for BAG1 targets androgen receptor-positive prostate cancer through oxidative stress signaling pathway. iScience 2022;25:104175.
29. Pan M, Solozobova V, Kuznik NC, Jung N, Grassle S, Gourain V, et al. Identification of an imidazopyridine-based compound as an oral selective estrogen receptor degrader for breast cancer therapy. Cancer Res Commun 2023;3:1378–96.
30. Abida W, Patnaik A, Campbell D, Shapiro J, Bryce AH, McDermott R, et al. Rucaparib in men with metastatic castration-resistant prostate cancer harboring a BRCA1 or BRCA2 gene alteration. J Clin Oncol 2020;38:3763–72.
31. Robinson D, Van Allen EM, Wu YM, Schultz N, Lonigro RJ, Mosquera JM, et al. Integrative clinical genomics of advanced prostate cancer. Cell 2015;161:1215–28.
32. Fenor de la Maza MD, Chandran K, Rekowski J, Shui IM, Gurel B, Cross E, et al. Immune biomarkers in metastatic castration-resistant prostate cancer. Eur Urol Oncol 2022;5:659–67.
33. Liberzon A, Birger C, Thorvaldsdottir H, Ghandi M, Mesirov JP, Tamayo P, et al. The molecular signatures database (MSigDB) hallmark gene set collection. Cell Syst 2015;1:417–25.
34. Bulusu KC, Tym JE, Coker EA, Schierz AC, Al-Lazikani B. canSAR: updated cancer research and drug discovery knowledgebase. Nucleic Acids Res 2014;42:D1040–7.
35. Coker EA, Mitsopoulos C, Tym JE, Komianou A, Kannas C, Di Micco P, et al. canSAR: update to the cancer translational research and drug discovery knowledgebase. Nucleic Acids Res 2019;47:D917–D22.
36. Patel MN, Halling-Brown MD, Tym JE, Workman P, Al-Lazikani B. Objective assessment of cancer genes for drug discovery. Nat Rev Drug Discov 2013;12:35–50.
37. de Groot BL, van Aalten DM, Scheek RM, Amadei A, Vriend G, Berendsen HJ. Prediction of protein conformational freedom from distance constraints. Proteins 1997;29:240–51.
38. Gotz R, Wiese S, Takayama S, Camarero GC, Rossoll W, Schweizer U, et al. Bag1 is essential for differentiation and survival of hematopoietic and neuronal cells. Nat Neurosci 2005;8:1169–78.
39. Irizarry RA, Hobbs B, Collin F, Beazer-Barclay YD, Antonellis KJ, Scherf U, et al. Exploration, normalization, and summaries of high density oligonucleotide array probe level data. Biostatistics 2003;4:249–64.
40. Dai M, Wang P, Boyd AD, Kostov G, Athey B, Jones EG, et al. Evolving gene/transcript definitions significantly alter the interpretation of GeneChip data. Nucleic Acids Res 2005;33:e175.

41. Neeb A, Figueiredo I, Gurel B, Rodrigues DN, Rekowski J, Riisnaes R, et al. Development and validation of a new BAG-1L specific antibody to quantify BAG-1L protein expression in advanced prostate cancer. Lab Invest 2023;103: 100245.
42. Taing L, Bai G, Cousins C, Cejas P, Qiu X, Herbert ZT, et al. CHIPS: a snakemake pipeline for quality control and reproducible processing of chromatin profiling data. F1000Research 2021;10:517.
43. Qiu X, Feit AS, Feiglin A, Xie Y, Kesten N, Taing L, et al. CoBRA: containerized bioinformatics workflow for reproducible ChIP/ATAC-seq analysis. Genomics Proteomics Bioinformatics 2021;19:652–61.
44. Li H, Durbin R. Fast and accurate short read alignment with burrows-wheeler transform. Bioinformatics 2009;25:1754–60.
45. Zhang Y, Liu T, Meyer CA, Eeckhoute J, Johnson DS, Bernstein BE, et al. Model-based analysis of ChIP-Seq (MACS). Genome Biol 2008;9:R137.
46. Kent WJ, Zweig AS, Barber G, Hinrichs AS, Karolchik D. BigWig and BigBed: enabling browsing of large distributed datasets. Bioinformatics 2010;26:2204–7.
47. Ramirez F, Ryan DP, Gruning B, Bhardwaj V, Kilpert F, Richter AS, et al. deepTools2: a next generation web server for deep-sequencing data analysis. Nucleic Acids Res 2016;44:W160–5.
48. Richards J, Lim AC, Hay CW, Taylor AE, Wingate A, Nowakowska K, et al. Interactions of abiraterone, eplerenone, and prednisolone with wild-type and mutant androgen receptor: a rationale for increasing abiraterone exposure or combining with MDV3100. Cancer Res 2012;72:2176–82.
49. Tym JE, Mitsopoulos C, Coker EA, Razaz P, Schierz AC, Antolin AA, et al. canSAR: an updated cancer research and drug discovery knowledgebase. Nucleic Acids Res 2016;44:D938–43.
50. Mitsopoulos C, Di Micco P, Fernandez EV, Dolciami D, Holt E, Mica IL, et al. canSAR: update to the cancer translational research and drug discovery knowledgebase. Nucleic Acids Res 2021;49:D1074–D82.
51. Andrews PR, Craik DJ, Martin JL. Functional group contributions to drug-receptor interactions. J Med Chem 1984;27:1648–57.
52. Shim JH, Xiao C, Hayden MS, Lee KY, Trombetta ES, Pypaert M, et al. CHMP5 is essential for late endosome function and down-regulation of receptor signaling during mouse embryogenesis. J Cell Biol 2006;172:1045–56.
53. Papadakis E, Robson N, Yeomans A, Bailey S, Laversin S, Beers S, et al. A combination of trastuzumab and BAG-1 inhibition synergistically targets HER2 positive breast cancer cells. Oncotarget 2016;7:18851–64.
54. Gil V, Miranda S, Riisnaes R, Gurel B, D'Ambrosio M, Vasciaveo A, et al. HER3 is an actionable target in advanced prostate cancer. Cancer Res 2021; 81:6207–18.
55. Welti J, Sharp A, Yuan W, Dolling D, Nava Rodrigues D, Figueiredo I, et al. Targeting bromodomain and extra-terminal (BET) family proteins in castration-resistant prostate cancer (CRPC). Clin Cancer Res 2018;24:3149–62.
56. Sowalsky AG, Figueiredo I, Lis RT, Coleman I, Gurel B, Bogdan D, et al. Assessment of androgen receptor splice variant-7 as a biomarker of clinical response in castration-sensitive prostate cancer. Clin Cancer Res 2022;28: 3509–25.
57. Andersen RJ, Mawji NR, Wang J, Wang G, Haile S, Myung JK, et al. Regression of castrate-recurrent prostate cancer by a small-molecule inhibitor of the amino-terminus domain of the androgen receptor. Cancer Cell 2010;17:535–46.
58. De Mol E, Fenwick RB, Phang CT, Buzon V, Szulc E, de la Fuente A, et al. EPI-001, a compound active against castration-resistant prostate cancer, targets transactivation Unit 5 of the androgen receptor. ACS Chem Biol 2016; 11:2499–505.
59. Leong AS, Leong TY. Standardization in immunohistology. Methods Mol Biol 2011;724:37–68.
60. Sfanos KS, Yegnasubramanian S, Nelson WG, Lotan TL, Kulac I, Hicks JL, et al. If this is true, what does it imply? How end-user antibody validation facilitates insights into biology and disease. Asian J Urol 2019;6:10–25.
61. Qiu X, Boufaied N, Hallal T, Feit A, de Polo A, Luoma AM, et al. MYC drives aggressive prostate cancer by disrupting transcriptional pause release at androgen receptor targets. Nat Commun 2022;13:2559.
62. Schiewer MJ, Knudsen KE. DNA damage response in prostate cancer. Cold Spring Harb Perspect Med 2019;9:a030486.
63. Ferraldeschi R, Nava Rodrigues D, Riisnaes R, Miranda S, Figueiredo I, Rescigno P, et al. PTEN protein loss and clinical outcome from castration-resistant prostate cancer treated with abiraterone acetate. Eur Urol 2015;67:795–802.
64. Mandigo AC, Shafi AA, McCann JJ, Yuan W, Laufer TS, Bogdan D, et al. Novel oncogenic transcription factor cooperation in RB-deficient cancer. Cancer Res 2022;82:221–34.
65. Tang CC, Shan LP, Wang WM, Lu G, Tare RS, Lee KKH. Generation of a Bag1 homozygous knockout mouse embryonic stem cell line using CRISPR/Cas9. Stem Cell Res 2017;21:29–31.
66. Clemo NK, Collard TJ, Southern SL, Edwards KD, Moorghen M, Packham G, et al. BAG-1 is up-regulated in colorectal tumour progression and promotes colorectal tumour cell survival through increased NF-kappaB activity. Carcinogenesis 2008;29:849–57.
67. Markowski MC, Wang H, De Marzo AM, Schweizer MT, Antonarakis ES, Denmeade SR. Clinical efficacy of bipolar androgen therapy in men with metastatic castration-resistant prostate cancer and combined tumor-suppressor loss. Eur Urol Open Sci 2022;41:112–5.
68. Leung JK, Tam T, Wang J, Sadar MD. Isolation and characterization of castration-resistant prostate cancer LNCaP95 clones. Hum Cell 2021;34:211–8.
69. Kilbas PO, Can ND, Kizilboga T, Ezberci F, Doganay HL, Arisan ED, et al. CRISPR/Cas9-mediated Bag-1 knockout increased mesenchymal characteristics of MCF-7 cells via Akt hyperactivation-mediated actin cytoskeleton remodeling. PLoS One 2022;17:e0261062.
70. Laccetti AL, Chatta GS, Iannotti N, Kyriakopoulos C, Villaluna K, Le Moigne R, et al. Phase 1/2 study of EPI-7386 in combination with enzalutamide (enz) compared with enz alone in subjects with metastatic castration-resistant prostate cancer (mCRPC). J Clin Oncol 41:6s, 2023 (suppl; abstr 179).
71. Pachynski RK, Iannotti N, Laccetti AL, Carthon BC, Chi KN, Smith MR, et al. Oral EPI-7386 in patients with metastatic castration-resistant prostate cancer. J Clin Oncol 41,6s, 2023 (suppl; abstr 177).